

Generation of Palaeocene Adakitic Andesites by Magma Mixing; Yanji Area, NE China

FENG GUO^{1,2*}, EIZO NAKAMURU², WEIMING FAN¹,
KATSURA KOBAYOSHI² AND CHAOWEN LI¹

¹KEY LABORATORY OF MARGINAL SEA GEOLOGY, GUANGZHOU INSTITUTE OF GEOCHEMISTRY, CHINESE ACADEMY OF SCIENCES, WUSHAN, GUANGZHOU, 510640, CHINA

²INSTITUTE FOR STUDY OF THE EARTH'S INTERIOR (ISEI), OKAYAMA UNIVERSITY, YAMADA 827, MISASA, TOTTORI 682-0193, JAPAN

RECEIVED JUNE 16, 2006; ACCEPTED DECEMBER 14, 2006;
ADVANCE ACCESS PUBLICATION FEBRUARY 2, 2007

Palaeocene (c. 55–58 Ma) adakitic andesites from the Yanji area, NE China, are typically clinopyroxene-bearing sodic andesites containing 60.9–62.2% SiO₂ and 4.02–4.36% MgO, with high Mg-number [100 Mg/(Mg + ΣFe) atomic ratio] from 65.5 to 70.1. Whole-rock geochemical features include high Cr (128–161 ppm) and Ni (86–117 ppm) concentrations, extremely high Sr (2013–2282 ppm), low Y (10–11 ppm) and heavy rare earth elements (HREE; e.g. Yb = 0.79–1.01 ppm), and mid-ocean ridge basalt (MORB)-like Sr–Nd–Pb isotopic compositions [e.g. ⁸⁷Sr/⁸⁶Sr(*i*) = 0.70298–0.70316, ε_{Nd}(*t*) = +3.8 to +6.3 and ²⁰⁶Pb/²⁰⁴Pb = 17.98–18.06], analogous to high-Mg adakites occurring in modern subduction zones. However, mineralogical evidence from clinopyroxene phenocrysts and microcrystalline plagioclase clearly points to magma mixing during magma evolution. Iron-rich clinopyroxene (augite) cores with low Sr, high Y and heavy REE contents, slightly fractionated REE patterns and large negative Eu anomalies probably crystallized along with low-Ca plagioclase from a lower crustal felsic magma. In contrast, high Mg-number clinopyroxene (diopside and endiopside) mantles and rims have higher Sr and lower HREE and Y concentrations, highly fractionated REE patterns (high La/Yb) and negligible Eu anomalies, similar to those found in adakites from subduction zones. The Yanji adakitic andesites can be interpreted as a mixture between a crust-derived magma having low Mg-number and Sr, and high Y and HREE, and a mantle-derived high Mg-number adakite having high Sr and low Y and HREE concentrations. During storage and/or ascent, the mixed magma experienced further crustal contamination to capture zircons, of a range of ages, from the wall rocks. The absence of coeval arc magmatism and an extensional

tectonic regime in the Yanji area and surrounding regions suggest that these Palaeocene adakitic andesites were formed during post-subduction extension that followed the late Cretaceous Izanagi–Farallon ridge subduction. Generation of these adakitic andesites does not require contemporaneous subduction of a young, hot oceanic ridge or delamination of eclogitic lower crust as suggested by previous models.

KEY WORDS: magma mixing; adakitic andesites; Palaeocene; NE China

INTRODUCTION

High Mg-number [100Mg/(Mg + ΣFe) atomic ratio] andesites and their intrusive equivalents are a class of intermediate and felsic igneous rocks with Mg-number >45, a feature that distinguishes them from normal andesites that typify arc magmatism (e.g. Kay, 1978; Kelemen, 1995; Tatsumi, 2006). This characteristic suggests that some high Mg-number andesites might represent near-primary melts in equilibrium with the Earth's mantle (Kushiro, 1969; Hirose, 1997). The petrogenesis of high Mg-number andesite has been extensively studied because of its unique geochemical characteristics and geological significance (e.g. Kay, 1978; Rogers *et al.*, 1985; Yogodzinski *et al.*, 1995; Shimoda *et al.*, 1998; Wang *et al.*, 2002a; Tsuchiya *et al.*, 2005; Tatsumi, 2006). A variety of petrogenetic models have been proposed, including differentiation of high-Mg

*Corresponding author. Telephone: + 86-20-85290280. Fax: + 86-20-85290130. E-mail: guofengt@263.net

basalt (Wang *et al.*, 2002a), reaction between slab melt and the overlying mantle wedge (Yogodzinski *et al.*, 1995; Bindeman *et al.*, 2005; Tsuchiya *et al.*, 2005), and melt derivation from a lithospheric mantle metasomatized by silica-rich melt or fluid (e.g. high-Mg andesites and bajaites, Prouteau *et al.*, 2001; Hanyu *et al.*, 2002; Calmus *et al.*, 2003; Martin *et al.*, 2005; Tatsumi, 2006). Most 'arc andesites', in contrast, are derived from basaltic magmas via complex and variable processes such as fractional crystallization, crustal contamination, anatexis of pre-existing basaltic crust, and magma mixing. Although high Mg-number andesites have rather primitive compositions, they also show many compositional similarities to bulk continental crust, a geochemical reservoir highly enriched in incompatible elements. Indeed, it has been suggested that the petrogenesis of these rocks could have been an important crust-forming process in the early Earth (Kelemen, 1995; Rudnick & Fountain, 1995; Taylor & McLennan, 1995).

Many adakites, which are andesitic to dacitic rocks formed at modern subduction zones, also have high Mg-number as well as high Sr, low Y and heavy rare earth element (HREE) concentrations and highly fractionated REE patterns (e.g. Kay, 1978; Rogers *et al.*, 1985; Saunders *et al.*, 1987; Defant & Drummond, 1990; Kay *et al.*, 1993; Yogodzinski *et al.*, 1995; Stern & Kilian, 1996). Using a database comprising >340 analyses of adakites in modern subduction zones, Martin *et al.* (2005) summarized and classified modern adakites into two subgroups: high-SiO₂ and low-SiO₂. They further proposed that the low-SiO₂ adakites, like bajaites from Baja California, Adak-type magnesian andesites from the Aleutian and Andean Arcs, and probably also Archaean sanukitoids, owe their high Mg-number, Sr, Cr and Ni, and low Y and HREE concentrations to derivation from incompatible element enriched mantle that was metasomatized by high-pressure slab melts. High-SiO₂ adakites, in contrast, are considered to be produced by reactions between high-pressure slab melts and the overlying mantle wedge, and typically range to lower MgO, Mg-number, Cr and Ni (e.g. Kay, 1978; Rogers *et al.*, 1985; Defant & Drummond, 1990; Yogodzinski *et al.*, 1995; Calmus *et al.*, 2003; Martin *et al.*, 2005; Xiong *et al.*, 2006). The andesites of the Yanji area, which form the focus of the present study, are compositionally similar to low-SiO₂ adakites except for their higher SiO₂ (>60%) (Martin *et al.*, 2005). However, they were produced in a post-subduction tectonic setting with no contemporaneous subduction of young, hot oceanic lithosphere. These rocks are not strictly adakites as originally defined by Defant & Drummond (1990), and so we refer to them here as the Yanji 'adakitic andesites'.

Because of the near primary compositions of many adakites and high Mg-number andesites, many previous studies have concentrated mainly on their geodynamic

significance (slab melt–mantle reaction, melt metasomatism and crustal growth, etc.) rather than on processes that might influence the compositional evolution of the parental magmas. However, ion microprobe analyses of clinopyroxene phenocrysts in 'primitive' adakites from the Aleutian Arc suggest that magma mixing occurred during magma ascent (Yogodzinski & Kelemen, 1998). Also, some adakites from the Austral volcanic zone (e.g. at Cerro Pampa and Cook Island) have experienced crustal contamination or assimilation via fractional crystallization (AFC) processes (e.g. Kay *et al.*, 1993; Stern & Kilian, 1996; Motoki *et al.*, 2003). In addition, Macpherson *et al.* (2006) proposed that some adakites from Mindanao in the Philippines were produced through high-pressure fractional crystallization of arc basalts. Such studies suggest that the magmatic evolution of many adakites and other high Mg-number andesites might be far from simple and this needs to be carefully examined before the petrogenetic or geodynamic significance of these rocks can be fully appreciated.

In this paper, we present geochronological [Ar–Ar dating and sensitive high-resolution ion microprobe (SHRIMP) zircon U–Pb dating results], mineral (major and trace element) and whole-rock geochemical and isotopic (Sr–Nd–Pb and zircon Hf isotope) data from Palaeocene adakitic andesites from the Yanji area of NE China. The study is primarily focused on the processes that control the magmatic compositional evolution. Despite retaining Mg-number as high as 70, these rocks preserve evidence for magma mixing between a mantle-derived melt and an andesitic–dacitic melt produced by melting of the lower crust.

The time of subduction of the Pacific plate and its effect on the tectonic evolution of the East Asian continental margin has been long debated. Another aim of this study is to investigate possible links between the adakitic magmatism and the subduction of the Pacific plate, which began to subduct beneath the East Asian continental margin at ~100 Ma according to palaeomagnetic observations on the Pacific Ocean and its neighbouring Eurasia continents (Engelbreton *et al.*, 1985; Northrup *et al.*, 1995).

GEOLOGICAL BACKGROUND

Northeastern Asia comprises a series of accretionary orogens between the North China Block and Siberian Craton and the Pacific plate (Fig. 1a, Maruyama *et al.*, 1989; Sengör *et al.*, 1993). The history of tectonic evolution includes: (1) the subduction of the Palaeo-Asian Ocean from the early Palaeozoic to the early Mesozoic to form the Central Asian Orogenic Belt; (2) northwestward subduction of the Pacific plate controlling the evolution of the East Asian continental margin since the late Mesozoic. These multiple-stage plate interactions have

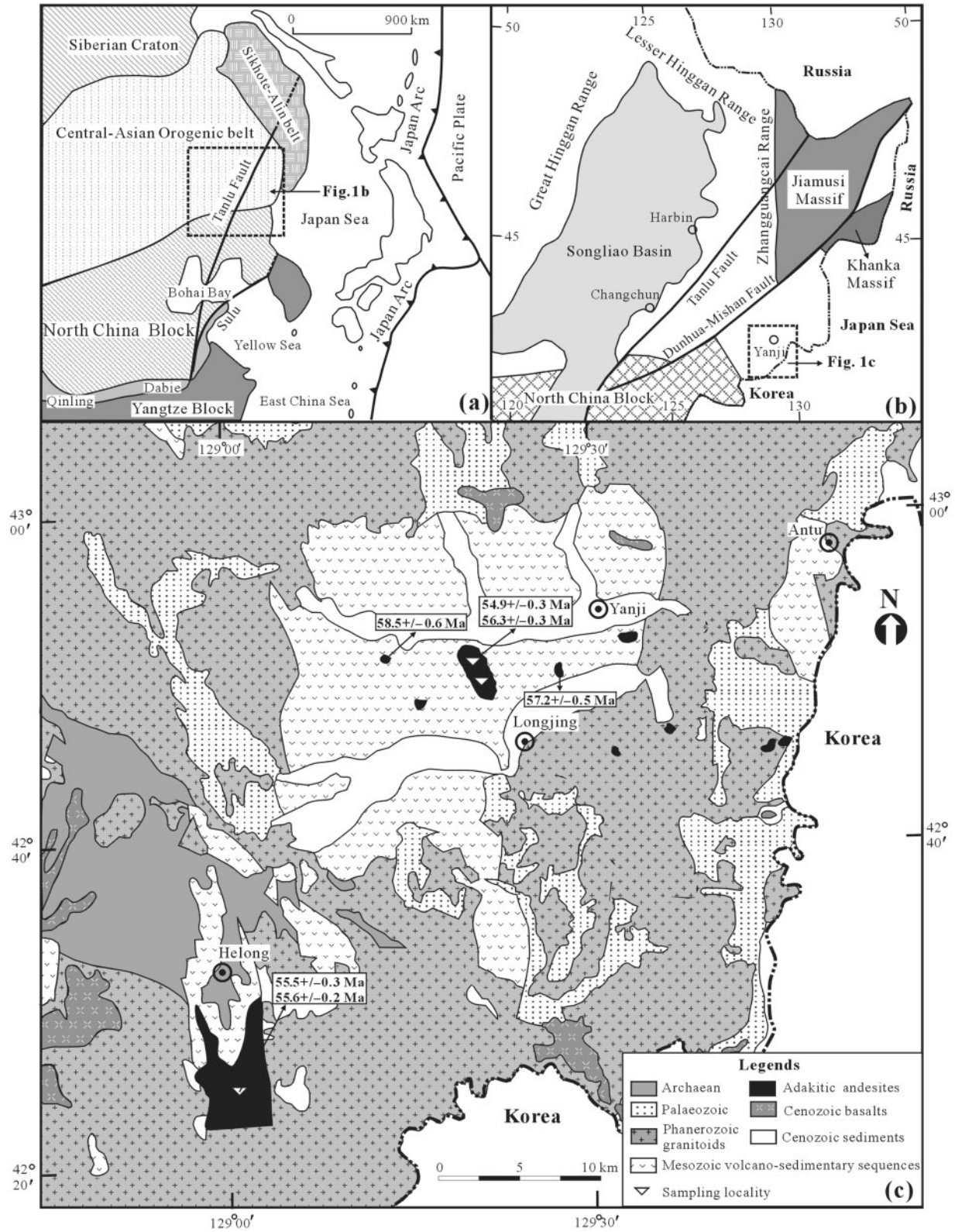


Fig. 1. (a) Tectonic divisions of NE Asia, modified after Maruyama *et al.* (1989); (b) tectonic divisions of NE China, modified after Zhang *et al.* (2004); (c) a geological map showing the distribution and ages of adakitic andesites in the Yanji area. Ar-Ar ages of adakitic andesites (clinopyroxene-bearing amphibole-andesites) near Helong city are from Li *et al.* (2007).

led to periodic continental growth and tectono-magmatic events in the Phanerozoic.

The Yanji area is located at the border of China, Russia and Korea, about 100 km west of the Japan Sea. It was considered part of the orogenic collage between the North China Block in the south and the Jiamusi–Khanka Massifs in the NE (Fig. 1b; Peng & Su, 1997; Xiao *et al.*, 2003; Jia *et al.*, 2004; Zhang *et al.*, 2004). To the south, there occur Archaean (~2.5 Ga) greenschist- and amphibolite-facies metamorphosed granitic rocks (JBGMR, 1988).

Palaeozoic strata are widely distributed in the region, and these have undergone variable degrees of metamorphism and deformation. Previous studies suggested that these Palaeozoic rocks might form tectonic mélanges related to the accretion of the NE Asian continent (e.g. Shao & Tang, 1995). Phanerozoic granitoids are widely exposed over an area of more than 20 000 km² and occupy about 70% of the region. Available zircon U–Pb data indicated that emplacement of these Phanerozoic granitoids extended from late Palaeozoic (285 Ma) to early Cretaceous (116 Ma) times (Zhang *et al.*, 2004). Zhang *et al.* (2004) related the multi-stage granitoid emplacement events to the evolution of the eastern segment of the Central Asian Orogenic Belt. The Mesozoic geological evolution was characterized by the eruption of voluminous lavas, mainly in the early Cretaceous (118–106 Ma, our unpublished Ar–Ar ages), granitoid emplacement (Zhang *et al.*, 2004), and deposition of terrestrial sediments as a result of post-orogenic lithospheric extension (Wang *et al.*, 2002b; Fan *et al.*, 2003).

Regional evolution since the late Cretaceous was probably related to subduction of the Farallon–Izanagi and Kula–Pacific ridges toward the NE Asian continental margin (Engelbreton *et al.*, 1985; Faure & Natal'in, 1992; Northrup *et al.*, 1995; Taira, 2001; Wang *et al.*, 2002b). Subduction-related magmatism is observed in the south-western and northern Japan Arcs (Kinoshita, 1995; Maeda & Kagami, 1996; Taira, 2001). However, coeval arc magmatism is scarce in the Yanji area and in the surrounding regions, the only possible example being the sporadic extrusion of the Palaeocene Yanji adakitic andesites (Fig. 1c). In contrast to the rare magmatism in the Yanji area, voluminous Palaeocene tholeiitic to calc-alkaline basalts erupted in fault-rift basins around the Bohai Bay area (Fig. 1a) and along the Tan-Lu fault in response to lithospheric extension (Chen *et al.*, 1992; Liu, R. X., *et al.*, 1992; Liu, C. Q., *et al.*, 1994; Liu, J. Q., *et al.*, 2001; Xu *et al.*, 1995), suggesting a similar extensional regime during the extrusion of the adakitic andesites in the Yanji area.

Rifting of the northeastern margin of the Asian continent started at ~22 Ma and was followed by development of the Japan Sea basin, which separated from the Asian continent between 22 and 15 Ma (Nakamura *et al.*, 1990; Yamaji, 1990; Lee *et al.*, 1999; Taira, 2001).

Back-arc extension continued into the Quaternary, associated with the eruption of Cenozoic–Quaternary basaltic lavas in NE China (e.g. Basu *et al.*, 1991; Liu, R. X., *et al.*, 1992; Liu, C. Q., *et al.*, 1994; Liu, J. Q., *et al.*, 2001; Zhang *et al.*, 1995).

FIELD AND PETROGRAPHIC CHARACTERISTICS

The Palaeocene adakitic andesites of the Yanji area occur as low hills up to 0.5 km² in area and form a WNW–ESE-trending chain ~25 km long. The volcanic units show well-developed columnar joints, dip very shallowly (<10°), and overlie Upper Cretaceous (K₂, Longjing Formation) sediments. Rare crustal xenoliths occur in the volcanic rocks and include granodiorite, gneiss, metagabbro and amphibolite. Two types of adakitic andesites can be identified in the Yanji area: one contains only clinopyroxene phenocrysts (clinopyroxene-andesite); the other (e.g. the outcrop near Helong town, Fig. 1c) is an amphibole-andesite with predominantly amphibole phenocrysts and subordinate clinopyroxene phenocrysts.

The studied samples were collected from the largest outcrop of clinopyroxene-andesites, located about 10 km NW of Longjing town (Fig. 1c). These rocks are fresh, with ~10% clinopyroxene phenocrysts up to 10 mm in size. The groundmass consists mainly of fine-grained (<0.5 mm) plagioclase, clinopyroxene and opaque oxides. Clinopyroxene is typically euhedral to subhedral (Fig. 2). In addition to the weakly zoned clinopyroxene (as shown in Fig. 2a), many clinopyroxene phenocrysts show complex zonation with plagioclase inclusions (Fig. 2b). In some clinopyroxene phenocrysts, orthopyroxene inclusions can also be found (Fig. 3).

ANALYTICAL TECHNIQUES

Major element compositions of minerals were determined using a JXA-8100 electron microprobe at Guangzhou Institute of Geochemistry, Chinese Academy of Sciences (CAS). An accelerating voltage of 15 kV, a specimen current of 3.0×10^{-8} A, and a beam size of 2 µm were employed. The analytical errors are generally less than 2%.

Trace element compositions of minerals (clinopyroxene and zircon) were analyzed by secondary ion mass spectrometry (SIMS) at the Pheasant Memorial Laboratory of the Institute for Study of the Earth's Interior (ISEI), Okayama University, Japan, using a Cameca ims-5f system. Analytical methods were similar to those used by Nakamura & Kushiro (1998). A primary negative oxygen beam of 10 nA intensity was used to sputter samples. The spot sizes were about 10 µm. Secondary ions were collected using a 4500 V accelerating voltage and measured by ion counting. To reduce the mass

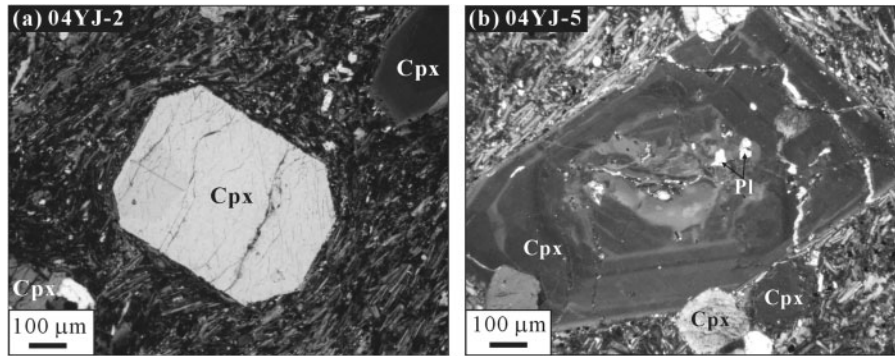


Fig. 2. Representative photographs of the clinopyroxene-andesites in the Yanji area. (a) Weakly zoned clinopyroxene; (b) complexly zoned clinopyroxene with plagioclase inclusions.

interference effect, -45 V of sample offset voltage was applied. The calculation factors for clinopyroxene and zircon were obtained by repeatedly analyzing standard clinopyroxenes from KLB-1 and SAG30 mantle peridotites and standard Sri Lanka zircon, respectively. Analytical errors (RSD%) were between 5 and 10% (1σ).

Argon step-heating analyses on one whole-rock sample (04YJ-3) were performed at the Institute of Geology and Geophysics, CAS on a GV5400 mass spectrometer operating in static mode. Samples were firstly crushed to 40–60 mesh, and fresh matrix, free of phenocrysts, was handpicked under a binocular microscope. The detailed analytical technique and age correction method were reported by Wang *et al.* (2004). The reference age for the GA-1550 biotite standard is 98.79 ± 0.96 Ma (Renne *et al.*, 1998). Ca and K correction factors were calculated from the CaF_2 and K-glass monitors: $(^{36}\text{Ar}/^{37}\text{Ar})_{\text{Ca}} = 2.6088 \times 10^{-4} \pm 1.1418 \times 10^{-5}$, $(^{39}\text{Ar}/^{37}\text{Ar})_{\text{Ca}} = 7.236 \times 10^{-4} \pm 2.814 \times 10^{-5}$, $(^{40}\text{Ar}/^{39}\text{Ar})_{\text{K}} = 2.648 \times 10^{-2} \pm 2.254 \times 10^{-4}$. Three other samples for Ar–Ar dating were analyzed using a GV5400 Ar mass spectrometer attached to a MIR10 CO_2 laser at Guangzhou Institute of Geochemistry, CAS. The laser beam is around 3 mm in diameter. A detailed description of the analytical technique was reported by Qiu (2006). The Ca and K correction factors are: $(^{38}\text{Ar}/^{36}\text{Ar})_{\text{a}} = 0.1869$, $(^{38}\text{Ar}/^{37}\text{Ar})_{\text{Ca}} = 0$, $(^{36}\text{Ar}/^{37}\text{Ar})_{\text{Ca}} = 2.69 \times 10^{-4}$, $(^{39}\text{Ar}/^{37}\text{Ar})_{\text{Ca}} = 7.09 \times 10^{-4}$, $(^{40}\text{Ar}/^{39}\text{Ar})_{\text{K}} = 0.00165$. The measured Ar–Ar results were processed using ArArCALC ver2.2c software (Koppers, 2002). The biotite standard ZBH2506 yields an Ar–Ar plateau age of 132.5 ± 0.20 Ma.

Zircon U–Pb dating was conducted using a sensitive high-resolution ion microprobe (SHRIMP II) at the Beijing SHRIMP Laboratory, Institute of Geology, Chinese Academy of Geological Science. Zircons were concentrated from fresh rock samples following normal separation methods, and were then handpicked and mounted together with standard TEM (417 Ma) onto

double-sided adhesive tape and enclosed in epoxy resin discs. The discs were polished, so as to effectively section the zircons nearly in half, and then cleaned, photographed and gold coated. Cathodoluminescence (CL) images were made on zircons prior to U–Pb analyses to reveal the internal textures and to guide the SHRIMP analyses. Analytical spot size averaged ~ 30 μm and each spot was rastered over 120 μm for 3 min to remove common Pb on the surface of the zircon. More detailed analytical procedures have been described by Compston *et al.* (1984, 1992), Williams (1998) and Liu *et al.* (2003). Decay constants used are those recommended by Steiger & Jäger (1977), and common Pb correction used the ^{204}Pb methods of Compston *et al.* (1984). The SHRIMP analytical data presented here are the mean values of five consecutive scans for each analytical spot. Errors are 1σ , whereas the weighted mean ages of samples are quoted at the 2σ level. The $^{206}\text{Pb}/^{238}\text{U}$ age is adopted in this study, as it is considered the most reliable measurement for concordant Phanerozoic zircons (Compston *et al.*, 1992).

Whole-rock major and trace element analyses were performed at Guangzhou Institute of Geochemistry, CAS, by X-ray fluorescence (XRF) spectrometry (Rigaku RIX-3000) and inductively coupled plasma mass spectrometry (ICP-MS), respectively. For major elements, the analytical errors are less than 2%. The analytical procedure for trace element determination was described by Liu *et al.* (1996). Precision for REE and high field strength elements (HFSE) is estimated to be 5% and about 10% for other elements from repeatedly analyzed US Geological Survey (USGS) standards BHVO-1 (basalt) and W-2 (diabase). The measured values for the standards were listed by Xu (2002).

Sr, Nd and Pb isotopic analyses were performed at Institute of Geology and Geophysics, CAS, on a MAT 262 mass spectrometer. Rock chips (< 20 mesh) were leached in purified 0.1 N HCl for 24 h at room temperature

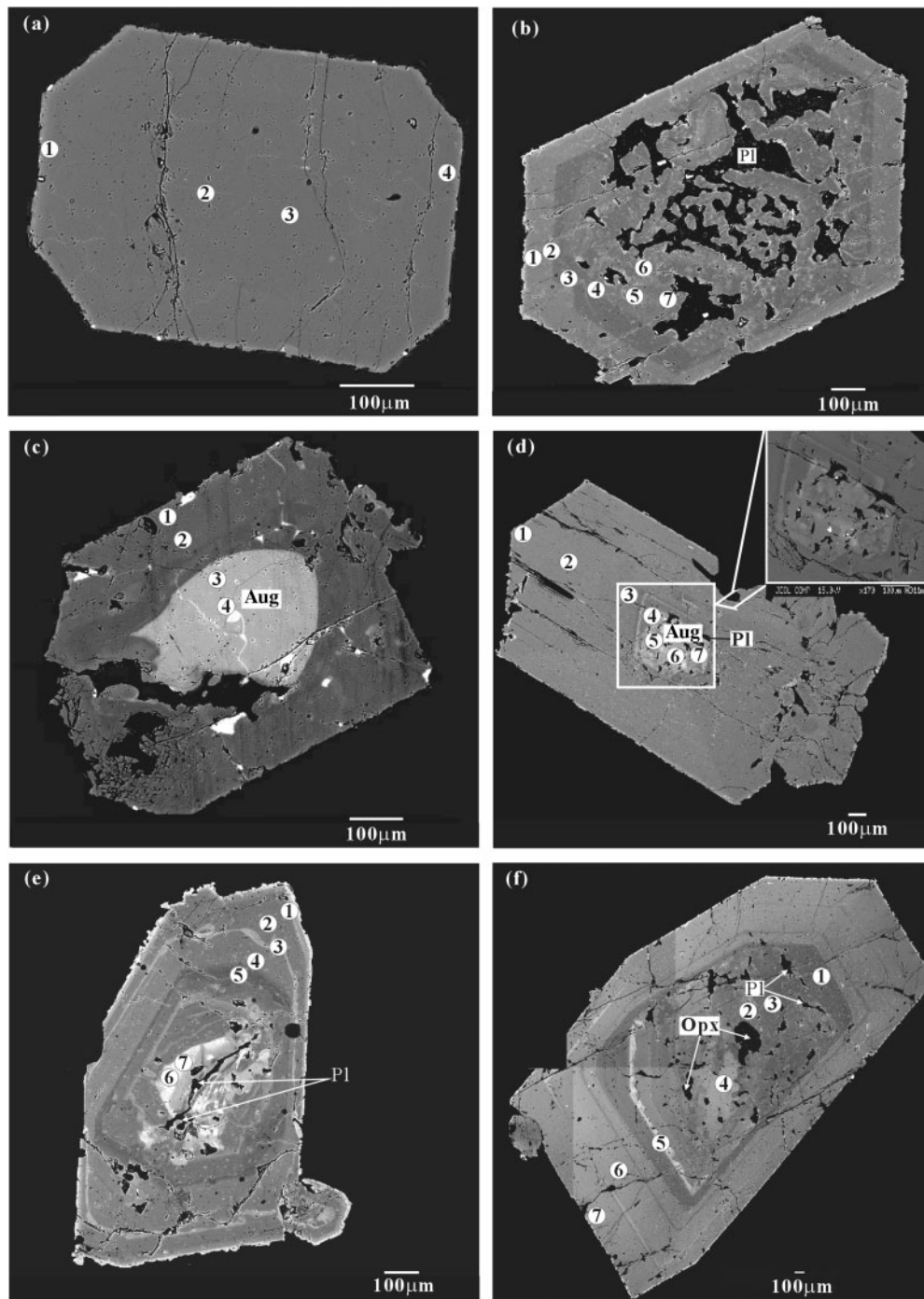


Fig. 3. Representative back-scattered electron images of clinopyroxene phenocrysts from the Yanji adakitic andesites, NE China. (a) Weakly zoned clinopyroxene; (b) normally zoned clinopyroxene with sieve structure in the core; (c) reversely zoned clinopyroxene with augite component at the core; (d) reversely zoned clinopyroxene with plagioclase inclusions; (e) complexly zoned clinopyroxene with reverse zonation from core to mantle, followed by oscillatory zonation; (f) complexly zoned clinopyroxene with orthopyroxene and plagioclase inclusions. Pl, plagioclase; Opx, orthopyroxene; Aug, augite.

to avoid the influence of surface alteration or weathering, especially for Sr and Pb isotopes. Powders were dissolved in HF–HClO₄ for Sr and Nd isotope analyses, and in HF–HNO₃ for Pb isotope analysis. Dissolution was

at 200°C for 1 week. Detailed analytical and correction techniques were described by Chen *et al.* (2002). The procedure blanks were <200 pg for Sr, <50 pg for Pb, and ~30 pg for Nd. Pb standard NBS 981 was used to

determine thermal fractionation, and the measured isotopic ratios of samples were corrected with a value of 0.11‰ per atomic mass unit. $^{86}\text{Sr}/^{88}\text{Sr}$ ratios were normalized to $^{86}\text{Sr}/^{88}\text{Sr} = 0.1194$ and $^{146}\text{Nd}/^{144}\text{Nd}$ ratios were normalized to $^{146}\text{Nd}/^{144}\text{Nd} = 0.7219$. The Ames standard yielded $^{143}\text{Nd}/^{144}\text{Nd} = 0.512149 \pm 3$ ($n = 98$) and NBS 987 gave $^{87}\text{Sr}/^{86}\text{Sr} = 0.710244 \pm 4$ ($n = 100$) for the last period of 6 months. Analytical errors for Sr, Nd and Pb isotopic ratios are given as 2σ . The $^{87}\text{Rb}/^{86}\text{Sr}$, $^{147}\text{Sm}/^{144}\text{Nd}$, U/Pb and Th/Pb ratios were calculated using the Rb, Sr, Sm, Nd, U, Th and Pb abundances obtained by ICP-MS. The initial Sr, Nd and Pb isotopic ratios were corrected using the Ar–Ar age of 55 Ma.

Hf isotope ratios were analyzed on zircon with a Neptune laser ablation multi-collector ICP-MS system attached to a Geolas 193 nm CQ ArF excimer laser system at the Institute of Geology and Geophysics, CAS. Analyses reported here were carried out with a laser beam diameter of 63 μm . The isobaric interference of ^{176}Yb on ^{176}Hf was corrected using a laboratory-established formula: $\beta_{\text{Yb}} = 0.8725\beta_{\text{Hf}}$. A detailed description of the zircon Hf isotope analytical technique has been given by Griffin *et al.* (2002) and Xu *et al.* (2004). Twenty-five analyses of standard zircon 95100 gave a $^{176}\text{Hf}/^{177}\text{Hf}$ ratio of 0.282665 ± 13 ($n = 25$). The $^{176}\text{Hf}/^{177}\text{Hf}$ ratios for sample zircon grains were corrected using the ratio obtained from standard 95100. The $^{176}\text{Lu}/^{177}\text{Hf}$ and $^{176}\text{Hf}/^{177}\text{Hf}$ ratios for chondrites are 0.0332 and 0.282772, respectively, and λ is $1.865 \times 10^{-11} \text{ year}^{-1}$.

MINERAL CHEMISTRY

Clinopyroxene

Clinopyroxene is the only phenocryst in the studied adakitic andesites. It is pale green with an euhedral to subhedral shape (Fig. 3a–f). Representative electron microprobe and ion microprobe analyses for clinopyroxene are listed in Table 1. They span a large range in SiO_2 (50.6–55.5%) and MgO (11.85–18.9%) contents and in Mg-number (66.2–94.0). Most clinopyroxene crystals are diopside and endiopside (Fig. 4) with relatively high Mg-number (>80); however, the bright cores seen in the back-scattered electron (BSE) images (Fig. 3c) are Fe-rich augite.

Geochemical data from a wide range of rock types show that clinopyroxenes from peridotite xenoliths, ophiolites, basalts, high-Mg andesites, gabbros and granulites can be roughly discriminated using a Mg-number vs Na_2O diagram (Fig. 5a). Compared with clinopyroxene from basaltic rocks, clinopyroxenes from peridotites have a high Mg-number. Clinopyroxenes from boninites are depleted in Na_2O , and those from high-Mg andesites have relatively low Na_2O and high Mg-number extending to the field for clinopyroxene in peridotites. Clinopyroxenes from the Yanji adakitic andesites have Mg-number and Na_2O contents comparable with those in high-Mg

andesites from modern subduction zones (Fig. 5b), except for the Fe-rich augite cores shown in Fig. 3c, which have high Na_2O (0.79%) and very low Mg-number (~ 66) and plot well away from the field for high-Mg andesites.

Most clinopyroxene phenocrysts in the Yanji adakitic andesites exhibit compositional zonation (Fig. 3a–f). Four types of clinopyroxene phenocrysts can be identified based on BSE imagery (Fig. 3): weakly, normally, reversely and complex zoned phenocrysts.

Weakly zoned clinopyroxene

This type of clinopyroxene is euhedral (Figs 2a and 3a). Rims have relatively low Mg-number (79–84) and are augite with an Fs component >10 , whereas the core is composed of high-Mg number (Mg-number = 87–89) diopside and endiopside. Relative to the high Mg-number cores, rims have high incompatible element concentrations, and both rims and cores show similar primitive mantle-normalized trace element patterns, characterized by significant Nb, Zr and Ti depletion relative to REE and by very small Sr–Eu anomalies (Fig. 6a). Such major and trace element variations from core to rim are typical of normal magma differentiation during crystal overgrowth.

Normally zoned clinopyroxene

This type of clinopyroxene is also euhedral, with dark cores and light rims (Fig. 3b). The cores are high in Cr_2O_3 ($>0.5\%$) and NiO (0.17–0.23%) and have high Mg-number (>93), and are classified as Cr-diopside (Table 1). Rims have slightly lower MgO and SiO_2 . Both cores and rims show similar trace element patterns to the weakly zoned clinopyroxene, with higher incompatible element concentrations in the rim (Fig. 6b). Such major and trace element variations possibly reflect overgrowth around a xenocrystic clinopyroxene.

Reversely zoned clinopyroxene

This type of clinopyroxene is subhedral. The bright core shown in Fig. 3c has very low MgO (11.8%) and SiO_2 (50.7%), and high FeO ($\sim 12\%$), whereas the dark rim has higher MgO ($\sim 17\%$) and SiO_2 (53.5%), and lower FeO (4.5%). Relative to the dark rim, the bright core has much higher REE, Zr and Y but much lower Sr concentrations. In primitive mantle-normalized trace element diagrams, apart from the Nb, Zr and Ti depletion, the Fe-rich cores also show strong negative Sr and Eu anomalies with Eu/Eu^* about 0.30 (Fig. 6c and Table 1). This contrasts with the high-MgO rims, which have negligible negative Sr and Eu anomalies (Fig. 6c and Table 1). The core shown in Fig. 6d also shows a progressive outwards increase in REE content and decrease in Sr/Y, Nd/Yb_{CN} and Eu/Eu^* ratios (i.e. richer in Fe, higher REE concentrations but lower Sr/Y, Eu/Eu^* and Nd/Yb_{CN}). The core and mantle also exhibit very different

Table 1: Representative electron microprobe and ion microprobe data for clinopyroxene phenocrysts

Sample:	04YJ-07 (Fig. 3a)				04YJ-02 (Fig. 3b)					
Spot:	1	2	3	4	1	2	3	4	5	6
SiO ₂	50.60	53.17	54.13	53.67	53.81	54.19	54.07	54.71	54.40	54.58
TiO ₂	1.00	0.35	0.33	0.45	0.26	0.19	0.22	0.16	0.16	0.19
Al ₂ O ₃	3.09	2.01	1.15	2.02	1.15	1.19	1.37	0.97	0.88	1.23
Cr ₂ O ₃	0.00	0.26	0.16	0.24	0.28	0.14	0.56	0.40	0.31	0.61
FeO	7.29	4.16	3.92	4.39	4.18	4.06	3.40	2.09	2.04	2.28
CaO	20.87	20.41	20.67	21.35	21.84	20.80	20.84	22.93	22.77	22.97
MgO	14.79	17.15	17.70	16.62	17.41	17.70	17.81	17.34	17.75	17.10
MnO	0.21	0.06	0.06	0.14	0.09	0.04	0.07	0.07	0.06	0.02
NiO	0.02	0.03	0.04	0.07	0.00	0.09	0.10	0.17	0.23	0.21
K ₂ O	0.02	0.01	0.02	0.02	0.00	0.03	0.02	0.03	0.01	0.01
Na ₂ O	0.41	0.47	0.37	0.33	0.30	0.35	0.37	0.31	0.29	0.36
Total	98.31	98.09	98.53	99.31	99.32	98.76	98.83	99.17	98.89	99.55
Mg-no.	78.5	88.1	89.1	87.2	88.2	88.7	90.4	93.7	94.0	93.1
Wo	44.3	43.0	42.7	44.6	44.3	42.8	43.2	47.1	46.4	47.3
En	43.7	50.2	50.9	48.3	49.1	50.7	51.3	49.5	50.3	49.0
Fs	12.1	6.8	6.3	7.2	6.6	6.5	5.5	3.4	3.2	3.7
Sr	187	162	163	210	151	156	156	178	166	196
Y	10.5	6.8	7.5	9.1	6.6	7.5	7.0	3.4	3.5	2.9
Zr	14.6	6.9	7.2	13.9	6.4	7.3	7.2	5.9	4.8	5.3
Nb	0.10	0.06	0.06	0.10	0.06	0.06	0.05	0.11	0.19	0.14
Ba	0.15	0.29	0.08	0.17	0.26	0.36	0.58	0.58	0.16	0.59
La	3.53	1.91	2.06	3.14	1.74	1.83	1.88	1.24	1.17	1.44
Ce	16.21	9.55	10.55	15.21	8.89	9.12	8.90	6.16	5.50	6.85
Pr	3.39	2.02	2.06	3.00	1.76	1.96	1.83	1.23	1.16	1.23
Nd	20.13	12.37	12.84	18.08	11.67	12.46	10.91	7.71	7.08	8.08
Sm	5.49	3.24	3.23	4.73	3.16	3.33	3.26	1.69	1.91	2.01
Eu	1.36	0.96	1.04	1.33	0.90	0.92	0.83	0.48	0.60	0.57
Gd	3.23	2.16	2.50	3.33	2.18	2.41	2.30	1.25	1.00	1.53
Dy	2.73	1.92	1.66	2.17	1.60	1.90	1.49	0.75	0.99	0.71
Er	0.91	0.55	0.59	0.72	0.64	0.53	0.46	0.23	0.28	0.29
Yb	0.47	0.30	0.38	0.47	0.28	0.34	0.29	0.13	0.21	0.13
Lu	0.05	0.03	0.03	0.05	0.03	0.03	0.03	0.02	0.02	0.02
Hf	1.30	0.74	1.14	1.24	0.69	1.01	0.88	0.27	0.45	0.33
Sr/Y	17.8	23.7	21.7	23.1	22.7	20.8	22.2	52.4	47.0	68.0
Eu/Eu*	0.91	1.05	1.08	0.97	0.99	0.95	0.88	0.96	1.20	0.95
Nd/Yb _{CN}	15.4	14.8	12.3	14.1	15.3	13.3	13.9	22.3	12.2	22.2

Sample:	04YJ-02 (Fig. 3c)				04YJ-07 (Fig. 3d)						
Spot:	1	2	3	4	1	2	3	4	5	6	7
SiO ₂	51.89	53.30	50.78	50.64	54.52	54.76	54.41	54.17	52.43	52.84	52.43
TiO ₂	0.53	0.27	0.25	0.27	0.32	0.30	0.28	0.32	0.37	0.34	0.37
Al ₂ O ₃	2.45	1.76	2.97	2.93	0.96	1.34	1.30	1.82	1.76	2.46	1.76
Cr ₂ O ₃	0.08	0.15	0.03	0.06	0.11	0.10	0.12	0.46	0.09	0.31	0.09
FeO	4.72	4.07	10.90	10.82	4.57	4.27	4.11	3.39	6.13	6.03	6.13

(continued)

Table 1: Continued

Sample:	04YJ-02 (Fig. 3c)				04YJ-07 (Fig. 3d)						
Spot:	1	2	3	4	1	2	3	4	5	6	7
CaO	21.07	21.66	20.33	20.40	19.85	21.09	20.77	21.36	20.91	20.63	20.91
MgO	16.99	16.96	11.85	11.87	18.66	17.76	17.66	17.14	16.19	15.73	16.19
MnO	0.13	0.15	0.20	0.26	0.17	0.14	0.15	0.09	0.20	0.19	0.20
NiO	0.03	0.06	0.00	0.00	0.03	0.00	0.01	0.07	0.10	0.00	0.10
K ₂ O	0.02	0.01	0.03	0.02	0.00	0.02	0.01	0.01	0.00	0.02	0.00
Na ₂ O	0.36	0.41	0.79	0.79	0.15	0.40	0.36	0.41	0.38	0.49	0.38
Total	98.27	98.77	98.12	98.05	99.35	100.16	99.16	99.22	98.56	99.03	98.56
Mg-no.	86.5	88.2	66.0	66.2	88.0	88.2	88.6	90.1	82.5	82.3	82.5
Wo	43.5	44.7	44.8	45.0	40.2	42.9	42.8	44.6	43.4	43.7	43.4
En	48.8	48.7	36.4	31.4	52.6	50.3	50.6	49.8	46.7	46.3	46.7
Fs	7.6	6.6	18.8	18.6	7.2	6.8	6.6	5.5	9.9	10.0	9.9
Sr	185	172	20.3	23.2	164	169	168	137	109	58.8	111
Y	8.4	8.5	142.0	140.5	7.8	7.2	7.8	15.3	48.1	79.7	24.8
Zr	12.4	9.7	56.8	58.2	7.9	7.6	7.7	9.2	21.5	23.3	13.7
Nb	0.11	0.10	0.06	0.06	0.06	0.05	0.05	0.10	0.08	0.15	0.07
Ba	0.92	1.86	1.34	1.10	0.13	0.09	0.10	0.26	0.68	7.15	0.62
La	2.61	2.24	5.51	5.39	2.08	2.14	2.40	1.42	4.12	9.02	3.85
Ce	11.80	9.43	29.85	28.97	10.23	10.33	11.13	7.23	19.21	46.28	17.77
Pr	2.48	1.90	6.59	6.29	2.15	2.20	2.35	1.45	3.85	9.30	3.35
Nd	14.40	10.46	45.75	42.24	12.78	13.36	14.28	9.06	25.80	56.54	19.41
Sm	4.70	2.99	18.59	17.58	3.03	3.86	3.97	3.25	8.39	15.37	6.13
Eu	1.04	0.70	1.94	1.97	1.00	0.88	1.15	0.78	1.24	1.40	0.98
Gd	2.65	2.14	19.78	20.32	2.80	1.65	2.72	2.59	6.69	13.17	4.59
Dy	1.67	1.83	25.02	24.72	2.08	1.86	1.90	3.05	9.19	14.93	5.35
Er	0.71	0.56	8.82	8.72	0.65	0.62	0.70	1.09	3.10	5.18	1.74
Yb	0.36	0.33	5.79	5.58	0.39	0.37	0.45	0.63	1.82	3.12	1.06
Lu	0.03	0.03	0.60	0.64	0.04	0.02	0.03	0.07	0.25	0.37	0.11
Hf	1.43	0.97	12.90	13.87	0.98	0.69	0.77	1.42	4.09	7.01	2.38
Sr/Y	22.0	20.4	0.14	0.16	21.0	23.5	21.5	9.0	2.3	0.74	4.5
Eu/Eu*	0.82	0.80	0.31	0.32	1.03	0.91	1.01	0.79	0.49	0.29	0.54
Nd/Yb _{CN}	14.6	11.6	2.9	2.8	12.1	13.2	11.5	5.2	5.2	6.6	6.7

Sample:	04YJ-05 (Fig. 3e)							04YJ-5 (Fig. 3f)						
Spot:	1	2	3	4	5	6	7	1	2	3	4	5	6	7
SiO ₂	53.81	53.59	53.55	53.81	53.86	51.78	51.78	53.74	53.72	54.36	54.15	54.00	51.83	54.02
TiO ₂	0.42	0.22	0.25	0.42	0.21	0.40	0.40	0.22	0.19	0.22	0.26	0.22	0.45	0.22
Al ₂ O ₃	1.35	1.04	1.00	1.35	0.92	1.73	1.73	0.98	1.07	1.66	1.51	0.94	1.45	0.91
Cr ₂ O ₃	0.02	0.16	0.23	0.02	0.20	0.06	0.06	0.28	0.38	1.03	0.27	0.33	0.00	0.38
FeO	6.13	4.02	3.91	6.13	3.31	8.07	8.07	2.56	3.00	2.25	3.39	3.04	6.71	3.11
CaO	21.12	21.71	22.17	21.12	23.07	21.58	21.58	23.04	21.64	22.06	21.28	22.45	21.35	22.20
MgO	16.33	17.59	17.29	16.33	17.50	14.60	14.60	18.06	18.90	17.41	18.00	18.29	16.30	18.32
MnO	0.32	0.14	0.17	0.32	0.11	0.17	0.17	0.00	0.10	0.05	0.10	0.07	0.28	0.10
NiO	0.22	0.06	0.04	0.22	0.11	0.16	0.16	0.08	0.28	0.15	0.10	0.08	0.10	0.13
K ₂ O	0.02	0.00	0.01	0.02	0.00	0.02	0.02	0.00	0.00	0.02	0.02	0.02	0.01	0.01

(continued)

Table 1: Continued

Sample:	04YJ-05 (Fig. 3e)							04YJ-5 (Fig. 3f)						
Spot:	1	2	3	4	5	6	7	1	2	3	4	5	6	7
Na ₂ O	0.53	0.32	0.35	0.53	0.33	0.49	0.49	0.31	0.41	0.50	0.47	0.31	0.52	0.28
Total	100.26	98.85	98.97	100.26	99.62	99.05	99.05	99.28	99.70	99.69	99.53	99.74	98.99	99.68
Mg-no.	82.7	88.7	88.8	82.7	90.5	76.5	76.5	92.7	91.9	93.3	90.5	91.6	81.4	91.4
Wo	43.4	44.0	45.0	43.4	46.1	44.8	44.8	45.9	43.0	45.9	43.5	44.7	43.3	44.3
En	46.7	49.6	48.8	46.7	48.7	42.2	42.2	50.1	52.3	50.4	51.1	50.6	46.0	50.9
Fs	9.8	6.4	6.2	9.8	5.2	13.1	13.1	4.0	4.7	3.6	5.4	4.7	10.6	4.8
Sr	170	185	174	185	201	170	178	201	215	183	155	226	156	161
Y	17.1	7.7	6.9	10.5	4.7	83.5	92.8	1.8	2.3	6.7	3.4	1.6	7.2	6.7
Zr	32.8	9.8	7.3	20.4	6.5	18.1	19.5	3.5	3.1	11.9	5.1	3.1	6.6	6.5
Nb	0.09	0.06	0.05	0.04	0.10	0.04	0.04	0.10	0.12	0.25	0.22	0.21	0.05	0.07
Ba	0.80	0.12	0.07	0.09	0.31	0.37	0.22	0.51	0.20	0.31	0.24	3.85	0.46	0.67
La	5.15	2.12	2.07	3.93	1.99	2.37	2.79	0.97	0.99	1.84	0.98	0.97	2.15	1.63
Ce	24.06	10.13	9.72	18.60	9.46	14.12	15.45	4.26	4.66	8.96	4.48	4.24	10.05	7.34
Pr	4.51	2.06	2.08	3.71	1.86	3.66	4.06	0.89	0.93	1.90	1.03	0.90	2.19	1.60
Nd	28.91	12.89	12.64	23.59	11.41	27.35	29.26	5.63	5.84	11.69	5.61	4.96	12.79	9.84
Sm	7.94	3.69	3.70	6.14	3.22	12.74	15.66	1.35	1.28	3.11	1.47	1.27	3.29	2.78
Eu	1.85	0.93	0.99	1.67	0.77	1.45	1.83	0.43	0.42	1.04	0.57	0.41	1.01	0.83
Gd	6.43	2.32	2.60	4.09	2.17	12.47	14.85	0.76	1.09	2.44	1.48	0.91	2.30	1.94
Dy	3.67	1.76	1.73	2.67	1.10	17.41	19.97	0.59	0.62	1.56	0.74	0.46	1.68	1.41
Er	1.40	0.61	0.55	1.16	0.46	5.06	6.11	0.15	0.17	0.50	0.25	0.18	0.48	0.46
Yb	0.80	0.37	0.34	0.58	0.23	3.03	3.56	0.07	0.13	0.28	0.14	0.08	0.30	0.23
Lu	0.08	0.04	0.03	0.05	0.02	0.38	0.42	0.01	0.01	0.03	0.01	0.01	0.03	0.03
Hf	2.72	0.96	0.93	1.63	0.48	7.41	9.07	0.28	0.29	0.86	0.42	0.30	0.73	0.87
Sr/Y	10.0	24.0	25.1	17.6	42.4	2.0	1.9	109	93.2	27.5	45.6	138	21.7	24.0
Eu/Eu*	0.77	0.90	0.93	0.96	0.84	0.35	0.36	1.17	1.07	1.12	1.16	1.10	1.06	1.03
Nd/Yb _{CN}	13.1	12.5	13.4	14.7	17.8	3.3	3.0	27.8	16.3	15.0	14.6	22.9	15.4	15.5

Mg-number = $100\text{Mg}/(\text{Mg} + \Sigma\text{Fe})$; CN, chondrite-normalized value (Sun & McDonough, 1989). $\text{Eu}/\text{Eu}^* = \text{Eu}_{\text{CN}}/(\text{Sm}_{\text{CN}} * \text{Gd}_{\text{CN}})^{0.5}$.

trace element patterns (Fig. 6d), as observed in Fig. 6c. Such reverse zonations in clinopyroxene major and trace element compositions suggest magma mixing during clinopyroxene overgrowth.

Complex zoned clinopyroxene

Some clinopyroxene phenocrysts show complex zonation patterns as illustrated in Fig. 3e and f. From the core to the rim, these phenocrysts show a stage of reverse zonation following by oscillatory zonation. Like that in Fig. 6c, the Fe-rich core in Fig. 6e shows similar trace element patterns with slight REE fractionation and negative Sr and Eu anomalies. The higher Mg-number clinopyroxene corresponds to lower incompatible element concentrations, suggesting a normal magma differentiation trend. Nevertheless, there also occur Cr-diopside fragments with Cr₂O₃ up to 1.03% and NiO at 0.28% (spot 2 in

Fig. 3f, Table 1), as observed in spots 4–6 in Fig. 3b. It is possible that the Cr-diopside fragments with similar trace element features to other high Mg-number clinopyroxene were xenocrystic from mantle peridotite that had been metasomatized by slab melt.

Clinopyroxene phenocrysts from the Yanji adakitic andesites show positive correlations between Sr/Y, Eu/Eu*, Nd/Yb_{CN} and Mg-number (Fig. 7a–c), and between Sr and Nd/Yb (Fig. 7d). Such variations do not reflect normal magmatic differentiation but point to mixing between a high Mg-number melt having high Eu/Eu*, Sr/Y and Nd/Yb_{CN} and a low Mg-number magma characterized by lower Eu/Eu*, Sr/Y and Nd/Yb_{CN} (e.g. Yögodzinski & Kelemen, 1998). Two-component mixing calculations show that most analyzed spots plot exactly on or adjacent to the mixing curves with the proportion of the Fe-rich core <10%.

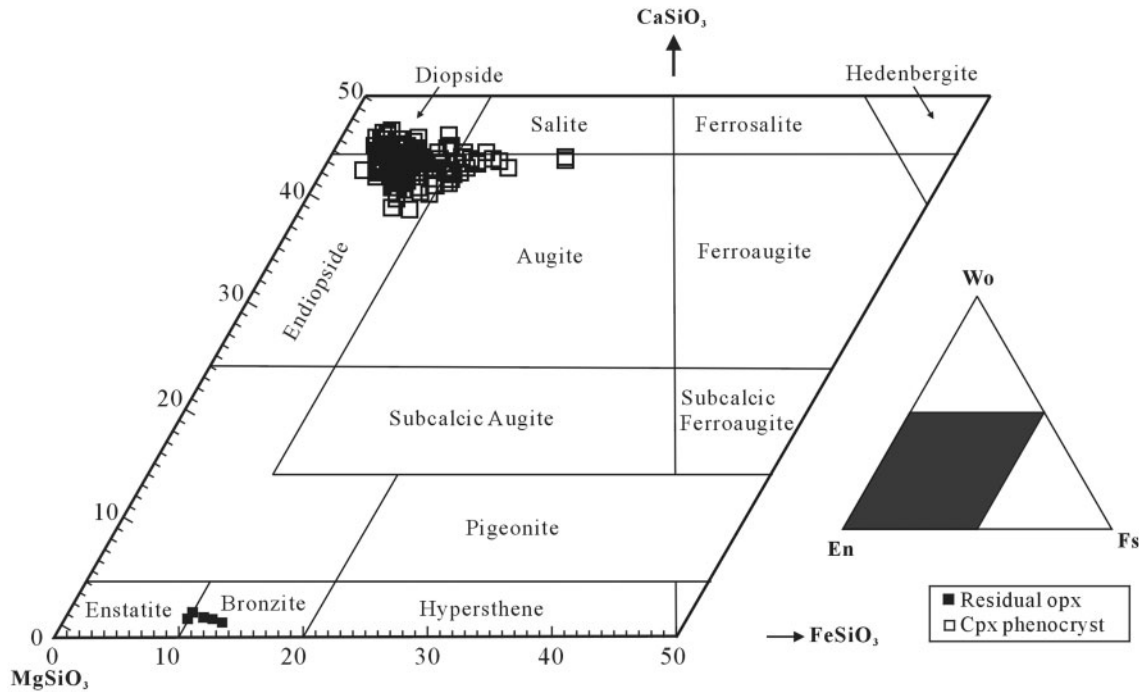


Fig. 4. CaSiO_3 – MgSiO_3 – FeSiO_3 diagram showing the compositions of pyroxene from the Yanji adakitic andesites, NE China. Most of the clinopyroxene phenocrysts classify as diopside and endiopside; the Fe-rich core is augite. Orthopyroxene inclusions are bronzite.

Analyses that plot away from the mixing lines were of clinopyroxenes that possibly crystallized during magmatic evolution (Fig. 7).

Orthopyroxene

Orthopyroxene phenocrysts are absent in the Yanji adakitic andesites. However, rare anhedral orthopyroxene crystals (0.2–0.5 mm) are enclosed in clinopyroxene phenocrysts (e.g. Fig. 3f). These have high SiO_2 (56.7–57.4%) and Mg-number (86.7–90.4), spanning an enstatite component range of 85.7–88.2, and are classified as bronzites in an Fs–En–Wo discrimination diagram (Table 2; Fig. 4).

Plagioclase

Plagioclase phenocrysts are also absent in the Yanji adakitic andesites. However, plagioclase forms the microcrystalline groundmass as well as anhedral inclusions in clinopyroxene phenocrysts (Fig. 3b, d, e and f). Groundmass plagioclase is labradorite, with an anorthite (An) content between 50.1 and 56.7, whereas plagioclase inclusions hosted in clinopyroxene phenocrysts are andesine, with lower An contents (31.2–43.1) (Table 3). Such compositional differences in plagioclase also contrast with normal magmatic differentiation trends, but like the reverse zonation patterns in the clinopyroxene phenocrysts are consistent with magma mixing during crystal growth.

GEOCHRONOLOGY AND ZIRCON REE CHEMISTRY

Ar–Ar dating results

Four samples (04YJ-3, 05YJ-1, 05YJ-20 and 05YJ-64) were selected for Ar–Ar dating to determine the eruption age of the Yanji adakitic andesites (see Fig. 1c). Samples 04YJ-3 and 05YJ-1 were collected from the same locality. 04YJ-3 was sampled from the upper part of the volcanic sequence and 05YJ-1 was sampled from the lower part. The whole-rock Ar–Ar analytical results are listed in Tables 4 and 5, and are shown in Fig. 8. Sample 04YJ-3 shows a flat age spectrum. During 11 of 14 consecutive steps (from 850°C to 1400°C), over 95% ^{39}Ar was released, defining a plateau age of 54.9 ± 0.3 Ma (2σ), consistent with an isochron age of 55.5 ± 0.4 Ma with $\text{MSWD} = 4.7$ ($n = 11$) (Fig. 8). The initial $^{40}\text{Ar}/^{36}\text{Ar}$ (287.3 ± 3.7) is consistent with that of atmosphere, precluding significant excess argon contamination (Fig. 8b). Thus, the plateau age of 54.9 ± 0.3 Ma can be interpreted as the minimum eruption age of the Yanji adakitic andesites. Sample (05YJ-1), from the base of the volcanic sequence, yields a plateau age of 56.3 ± 0.3 Ma (2σ), consistent with an isochron age of 55.9 ± 0.7 Ma with $\text{MSWD} = 0.81$ ($n = 13$) and initial $^{40}\text{Ar}/^{36}\text{Ar}$ at 301.9 ± 11.4 (Fig. 8c and d). These two ages are almost identical within the analytical errors.

The other two samples (05YJ-20 and 05YJ-64) also yield Palaeocene ages (Fig. 1). Sample 05YJ-20 yields a plateau

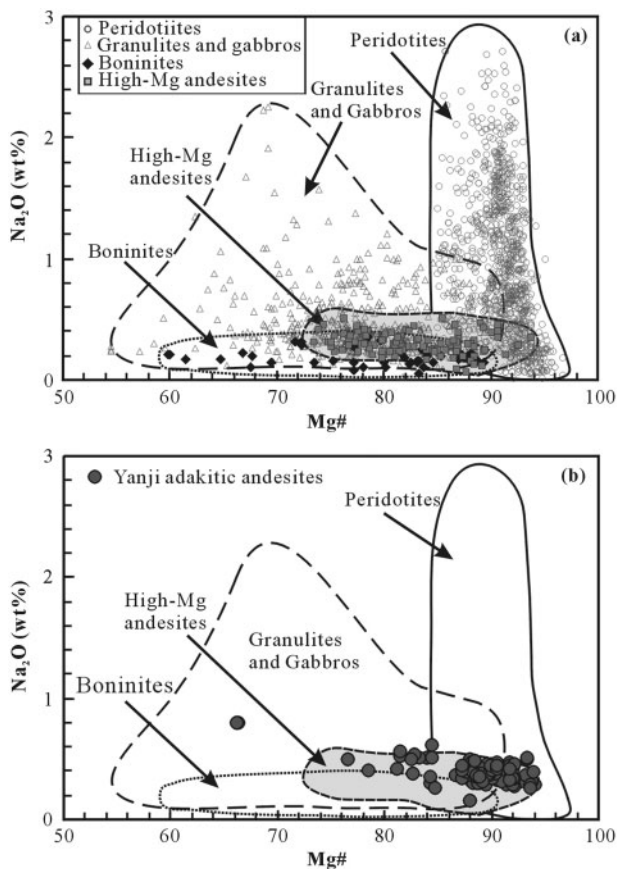


Fig. 5. Comparison of Mg-number and Na₂O contents of the Yanji adakitic andesites with clinopyroxene from different rock types, including peridotites, gabbros and granulites, boninites and high-Mg andesites. (a) Data compilation of clinopyroxene compositions for different rock types from: <http://georoc.mpch-mainz.gwdg.de/georoc/>. (b) The Yanji adakitic andesites (this study) show that most of the clinopyroxene phenocrysts have similar chemical composition to clinopyroxene from high-Mg andesites with relatively higher Mg-number and lower Na₂O than clinopyroxene from basaltic magmas, but they have higher Na₂O than those from boninites. Fe-rich clinopyroxene cores in Fig. 3c have higher Na₂O (0.79%) and lower Mg-number (66), very different from the other analyzed spots.

age of 57.2 ± 0.5 Ma and an isochron age of 56.3 ± 1.8 Ma (MSWD = 0.48, $n = 16$) (Fig. 8e and f). Sample 05YJ-64 gives a plateau age of 58.5 ± 0.6 Ma and an isochron age of 58.5 ± 2.3 Ma (MSWD = 0.08, $n = 14$) (Fig. 8g and h). The range of initial $^{40}\text{Ar}/^{36}\text{Ar}$ for both samples is well within the range of the atmosphere. Therefore, the two plateau ages are interpreted to represent the eruption age of the adakitic andesites.

In summary, the Ar–Ar dating results for the Yanji adakitic andesites give an eruption age of 55–58 Ma, corresponding to the Palaeocene epoch. These ages are consistent with the field observations that Upper Cretaceous sediments are entrained in, and interbedded with, the volcanic layers.

Zircon U–Pb dating results and REE chemistry

Zircon occurs as a very rare accessory in the Yanji adakitic andesites. The crystals are mostly clear, subhedral to euhedral stubby prisms, with length/width ratios about 1–3. They contrast with other volcanic zircons, which are usually slender prisms (Fig. 9a and b). Some CL images show core–mantle overgrowth relationships and oscillatory zoning textures, indicating a magmatic origin.

Twenty analyses of zircon span an apparent $^{206}\text{Pb}/^{238}\text{U}$ age range of 170–338 Ma (Table 6), much older than the Ar–Ar age of 55–58 Ma. When plotted on a $^{207}\text{Pb}/^{238}\text{U}$ vs $^{206}\text{Pb}/^{238}\text{U}$ diagram (Fig. 9c), they indicate a mean age of 190 ± 4 Ma with MSWD of 2.1 ($n = 14$). Except for one high-U and one high-Th zircon, the zircons have reasonably high Th/U ratios around 0.6 (Fig. 9d), also suggesting a magmatic origin. The mean age of 190 ± 4 Ma and the 170–338 Ma age range are comparable with the age range for granitoid intrusions in the region (e.g. Zhang *et al.*, 2004).

Trace element compositions of zircons from sample 04YJ-6 are listed in Table 7. The zircons of different ages show similar REE patterns with LREE depletion and HREE enrichment and significant positive Ce anomalies and negative Eu anomalies (Fig. 9e and f). Zircon crystals with an apparent $^{238}\text{U}/^{206}\text{Pb}$ age between 183 and 195 Ma have a Ce/Ce* range of 12.3–48.6 and a Eu/Eu* range of 0.19–0.27, except for one crystal (spot 13), which has a higher Eu/Eu* of 0.53. Other crystals with an apparent $^{238}\text{U}/^{206}\text{Pb}$ age either older than 200 Ma or younger than 180 Ma have a Ce/Ce* range of 11.4–44.6 and a Eu/Eu* range of 0.05–0.37.

The zircons span a large range of Y concentrations from 313 to 1777 ppm, but a narrow range of Hf concentrations from 2688 to 4632 ppm. Such features are very different from those of zircon populations from ultra-high pressure eclogites, which generally have low Y (<100 ppm) and high Hf (>9000 ppm) concentrations as well as smaller negative Eu anomalies (e.g. Rubatto, 2002). The high Y and low Hf concentrations, and significant negative Eu anomalies, suggest that the zircons in the Yanji adakitic andesites crystallized in the presence of plagioclase but not garnet.

GEOCHEMISTRY

Whole-rock major and trace elements

The studied Yanji adakitic andesites span a narrow range of SiO₂ from 60.9 to 62.2% and MgO from 4.02 to 4.36%, with a Mg-number range of 65.5–70.1 (Table 8). They have much higher MgO (and Mg-number) at given SiO₂ than experimental melts derived from metabasites (e.g. Rapp & Watson, 1995; Rapp *et al.*, 1999;

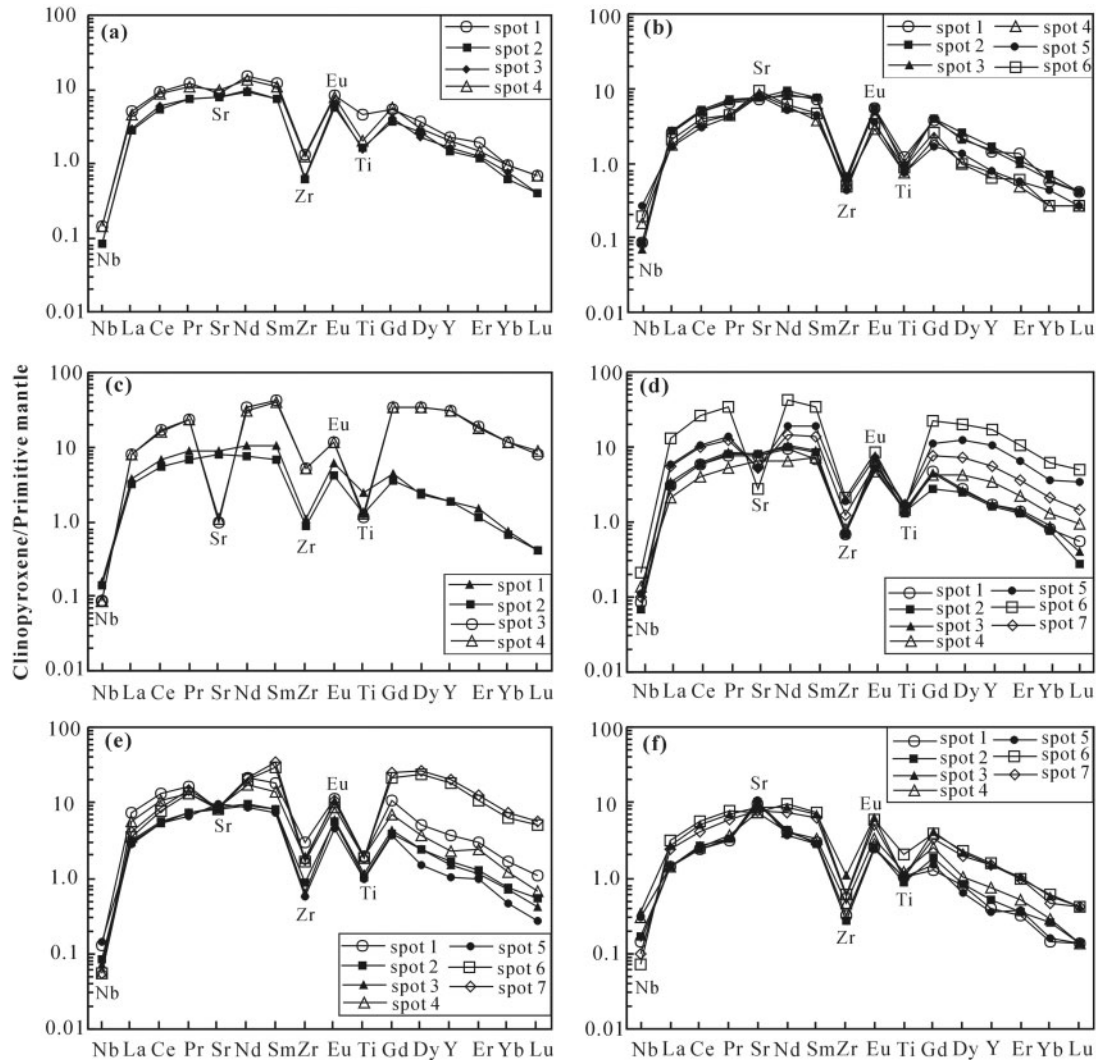


Fig. 6. Primitive mantle-normalized trace element patterns of clinopyroxene in the Yanji adakitic andesites. The sequence of diagrams corresponds to that of the back-scattered electron images in Fig. 3; trace element data are from Table 1. Primitive mantle values are from Sun & McDonough (1989).

Xiong *et al.*, 2005), but are similar to bajaites and high-Mg andesites and adakites in modern arcs such as the Japan and Aleutian Arcs and the Austral volcanic zone in South America (Fig. 10a; Kay *et al.*, 1993; Yogodzinski *et al.*, 1995; Stern & Kilian, 1996; Shimoda *et al.*, 1998; Calmus *et al.*, 2003; Tatsumi *et al.*, 2003; Tatsumi, 2006). Similarly, they also show rather high Cr (128–161 ppm) and Ni (86–117 ppm) concentrations, similar to those of bajaites from Baja California and high-Mg andesites and adakites in the Aleutian and Andean Arcs (Fig. 10b and c). A remarkable feature of the Yanji adakitic andesites is their extremely high Sr contents, from 2013 to 2282 ppm (Table 8), analogous to those of bajaites from Baja California and some Adak-type magnesian andesites from the Aleutian and Andean Arcs (Rogers *et al.*, 1985;

Saunders *et al.*, 1987; Kay *et al.*, 1993; Yogodzinski *et al.*, 1995; Stern & Kilian, 1996; Calmus *et al.*, 2003), but much higher than the Sr range of high-Mg andesites or diorites from the adjacent Japan Arc (Fig. 10d; Shimoda *et al.*, 1998; Kamei *et al.*, 2004; Tatsumi, 2006). In common with adakites from modern subduction zones (Defant & Drummond, 1990; Smithies, 2000; Martin *et al.*, 2005), the Yanji adakitic andesites also have low Y (10.4–11.0 ppm) and HREE concentrations (e.g. Yb is only 3–4 times chondritic values). Such features are reflected in a Y vs Sr/Y plot (Fig. 11), in which the Yanji adakitic andesites have Sr/Y values comparable with those of high Mg-number adakites and bajaites but much higher than those of the Japan Arc high-Mg andesites (e.g. Kamei *et al.*, 2004; Tatsumi, 2006).

Like adakites worldwide (e.g. Defant & Drummond, 1990; Yögozinski *et al.*, 1995; Martin *et al.*, 2005), the Yanji adakitic andesites show highly fractionated chondrite-normalized REE patterns (Fig. 12a), having a La/Yb range of 44–56 and negligible Eu anomalies ($\text{Eu}/\text{Eu}^* = 0.93\text{--}1.03$). Their primitive mantle-normalized trace element patterns are characterized by large ion lithophile element (LILE; Ba, Th, K, Pb and Sr) and LREE enrichment and Nb–Ta, P, Y and HREE depletion (Fig. 12b).

Whole-rock Sr–Nd–Pb isotope compositions

The measured and age-corrected Sr–Nd–Pb isotopic ratios of the studied Yanji adakitic andesites are given in Table 9. In general, these rocks have unradiogenic Sr [$^{87}\text{Sr}/^{86}\text{Sr}(i) = 0.70298\text{--}0.70316$] and radiogenic Nd [$\epsilon_{\text{Nd}(t)} = +3.8$ to $+6.3$] and Pb isotopic compositions ($^{206}\text{Pb}/^{204}\text{Pb}_i = 17.98\text{--}18.06$; $^{207}\text{Pb}/^{204}\text{Pb}_i = 15.49\text{--}15.55$, $^{208}\text{Pb}/^{204}\text{Pb}_i = 37.73\text{--}37.89$). Compared with modern

adakites and bajaites in subduction zones (e.g. Rogers *et al.*, 1985; Kay *et al.*, 1993; Yögozinski *et al.*, 1995; Stern & Kilian, 1996), the Yanji adakitic andesites have Sr–Nd isotopic compositions within the field of modern analogues but have lower Pb isotope ratios and plot within the array of global mid-ocean ridge basalt (MORB) (Fig. 13).

Compared with the early Cretaceous basalts in the region, the Yanji adakitic andesites have less radiogenic Sr and Pb, and more radiogenic Nd isotopic compositions (Fig. 13, our unpublished data). They have low T_{DM} , ranging from 284 to 442 Ma, much older than the eruptive age but overlapping the SHRIMP U–Pb age range for zircon in these rocks.

Zircon Hf isotope data

Hf isotopic ratios of zircons are listed in Table 10. The zircon crystals have positive $\epsilon_{\text{Hf}(t)}$ values ranging from $+2.0$ to 12.3 , with a mean of $+8.4$ (Fig. 14a).

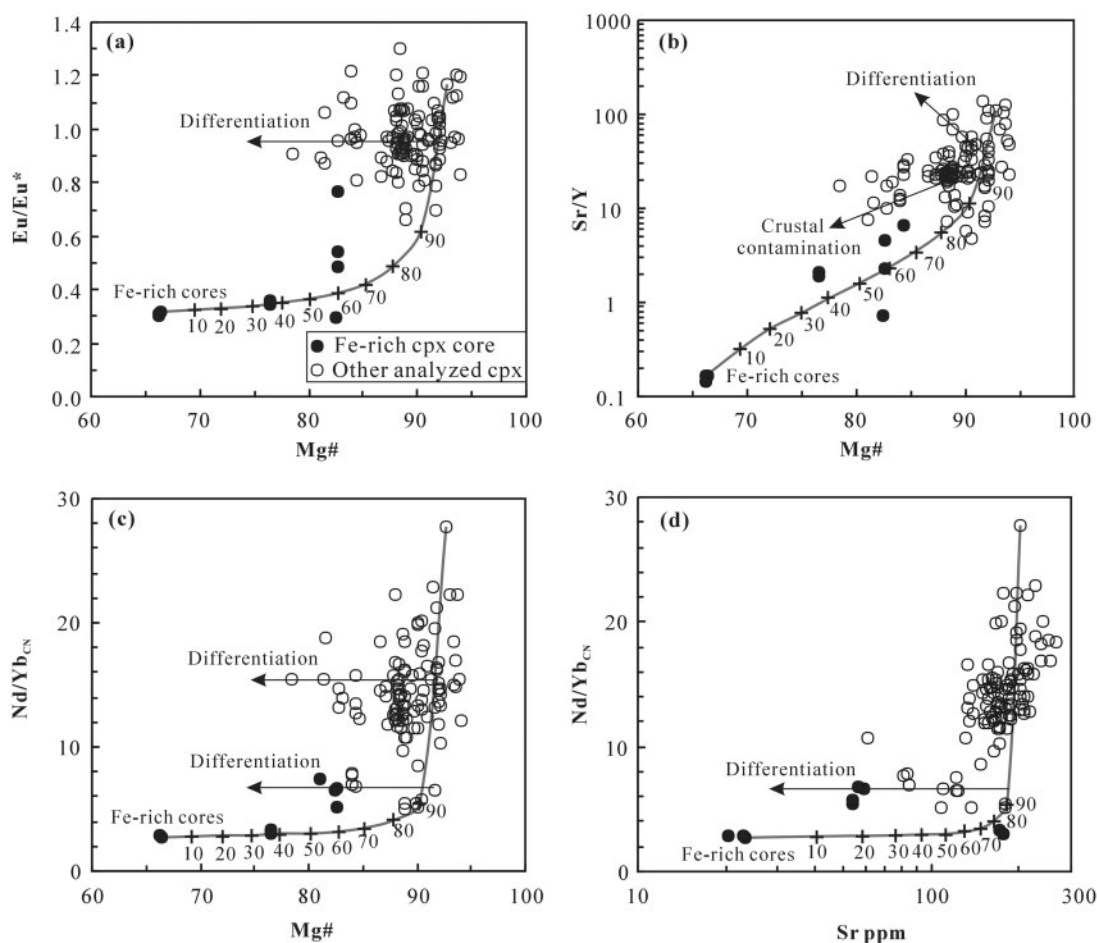


Fig. 7. Mg-number vs Eu/Eu^* (a), Sr/Y (b) and $\text{Nd}/\text{Yb}_{\text{CN}}$ (c), and Sr vs $\text{Nd}/\text{Yb}_{\text{CN}}$ (d) for clinopyroxene from the Yanji adakitic andesites, showing two-component mixing between a high Mg-number clinopyroxene with higher Eu/Eu^* , Sr/Y and $\text{Nd}/\text{Yb}_{\text{CN}}$ and a low Mg-number clinopyroxene with lower Eu/Eu^* , Sr/Y and $\text{Nd}/\text{Yb}_{\text{CN}}$ ratios. The continuous lines are mixing curves between the end-member components of clinopyroxene from spot 4 in Fig. 3c and spot 1 in Fig. 3f, respectively (see analytical data in Table 1). Numbers on the mixing curves represent the percentage of the high Mg-number clinopyroxene component. Arrows denote normal magma differentiation and crustal contamination trends. (See details in the text.)

Depleted mantle model Hf ages [$T_{DM}(Hf)$] range from 369 to 771 Ma, with a peak age at 400–500 Ma (Fig. 14b), slightly older than the whole-rock $T_{DM}(Nd)$.

The U–Pb zircon data resemble those of magmatic zircons from intermediate–felsic intrusions, whereas the zircon Hf isotope data suggest that the zircons crystallized from magmas that were derived from juvenile crustal materials.

Table 2: Representative electron microprobe analyses of orthopyroxene

Sample:	04YJ-5			04YJ-2	
	1	2	3	4	5
SiO ₂	56.84	57.41	57.63	57.08	56.71
TiO ₂	0.12	0.11	0.17	0.04	0.01
Al ₂ O ₃	1.66	1.35	1.54	1.60	1.44
Cr ₂ O ₃	0.11	0.13	0.03	0.04	0.00
FeO	6.48	7.32	6.58	8.10	9.06
MnO	0.12	0.13	0.09	0.05	0.16
CaO	1.26	0.96	1.07	0.84	0.55
MgO	33.96	33.21	33.52	32.83	32.95
NiO	0.33	0.12	0.26	0.26	0.17
Na ₂ O	0.03	0.08	0.08	0.03	0.05
K ₂ O	0.01	0.01	0.04	0.00	0.00
Total	100.93	100.84	101.00	100.86	101.11
Mg-no.	90.4	89.1	90.2	88.0	86.7
Wo	2.4	1.8	2.0	1.6	1.0
En	88.2	87.4	88.3	86.4	85.7
Fs	9.4	10.8	9.7	12.0	13.2

PETROGENESIS

In the following discussion, we focus on the constraints that mineral compositions place on magmatic processes and on the possible magma components involved in the petrogenesis of the Palaeocene Yanji adakitic andesites.

Mineralogical evidence for magma mixing

The complex compositional zonation of the clinopyroxene phenocrysts in the Yanji adakitic andesites suggest that these minerals experienced a complex overgrowth history. Most of the clinopyroxene phenocrysts experienced conditions that caused some degree of reverse zonation. Such a phenomena suggests that these clinopyroxene phenocrysts were neither products of a normal magmatic fractionation process nor were they produced by assimilation and fractional crystallization of a mafic magma, as both processes should result in normal zonation in the clinopyroxene. Reverse zonation can be formed as a result of a change in P – T conditions, magma mixing or by melt–mantle interaction, or by any combination of these processes.

P – T change?

High pressure will retard plagioclase fractionation, and in a hydrous andesitic magma, plagioclase will not crystallize when P is >20 kbar; in this case, the fractionating assemblage will be pyroxene + garnet + amphibole + quartz (Green, 1982). When T is $>1000^{\circ}\text{C}$ and $P > 5$ kbar, the fractionating phases include only clinopyroxene and orthopyroxene. If the common reverse zonation in clinopyroxene and the high An content in the microcrystalline groundmass plagioclase are a result of a P – T change, then a rapid increase in temperature of the

Table 3: Representative electron microprobe analyses of plagioclase

Sample:	04YJ-2				04YJ-5				04YJ-7				04YJ-9			
	inclusion in cpx		matrix		matrix		groundmass		inclusion in cpx		matrix		inclusion in cpx		matrix	
Spot:	1	2	3	4	5	6	7	8	9	10	11	12	13	14	15	16
SiO ₂	57.98	57.45	54.50	54.14	56.37	56.16	54.93	53.64	57.70	59.67	54.21	54.80	58.67	60.54	53.43	54.07
TiO ₂	0.05	0.09	0.06	0.07	0.08	0.10	0.07	0.05	0.04	0.03	0.05	0.08	0.06	0.06	0.05	0.02
Al ₂ O ₃	25.84	26.09	28.78	29.10	27.37	27.01	26.82	26.95	25.04	24.26	28.10	27.89	25.37	24.57	28.73	29.25
FeO	0.79	0.62	0.75	0.49	0.90	0.74	0.54	0.73	0.65	0.38	0.78	0.45	0.50	0.44	0.39	0.57
MgO	0.02	0.04	0.04	0.04	0.06	0.06	0.02	0.03	0.04	0.01	0.15	0.02	0.04	0.03	0.07	0.04
CaO	7.97	8.38	11.10	11.38	9.26	9.41	11.20	11.56	7.89	7.25	11.16	10.13	8.02	6.58	11.50	11.60
Na ₂ O	6.43	6.20	4.70	4.62	6.45	6.61	5.33	4.94	7.15	6.96	5.11	5.36	7.12	7.61	4.92	4.97
K ₂ O	0.36	0.38	0.19	0.27	0.46	0.49	0.35	0.28	0.50	0.90	0.20	0.33	0.41	0.60	0.25	0.24
Total	99.44	99.24	100.13	100.10	100.94	100.58	99.26	98.19	99.00	99.46	99.75	99.06	100.19	100.42	99.32	100.76
An	39.8	41.8	56.0	56.7	43.1	42.8	52.7	55.5	36.8	34.6	54.1	50.1	37.5	31.2	55.6	55.6
Ab	58.1	56.0	42.9	41.7	54.3	54.5	45.3	42.9	60.4	60.2	44.8	48.0	60.2	65.4	43.0	43.1
Or	2.2	2.3	1.1	1.6	2.5	2.7	2.0	1.6	2.8	5.1	1.1	2.0	2.3	3.4	1.4	1.4

Table 4: Whole-rock Ar–Ar dating of sample 04YJ-3 by step-heating

Step	T (°C)	Cumulative ³⁹ Ar	Atmosphere ⁴⁰ Ar (%)	³⁶ Ar/ ³⁹ Ar	³⁷ Ar/ ³⁹ Ar	³⁸ Ar/ ³⁹ Ar	⁴⁰ Ar/ ³⁹ Ar	⁴⁰ Ar/ ³⁶ Ar	Age (Ma)	±1σ
1	700	0.003	70.849	2.6600E-02	1.9480E+00	1.6010E-02	1.0910E+01	4.1010E+02	52.8	1.8
2	780	0.041	30.448	5.2830E-03	4.7460E-01	1.1890E-02	5.0330E+00	9.5280E+02	57.8	0.4
3	850	0.213	38.315	7.1730E-03	3.8590E-01	1.2950E-02	5.4810E+00	7.6410E+02	55.9	0.4
4	890	0.395	10.282	1.4330E-03	5.1630E-01	1.2250E-02	3.7580E+00	2.6220E+03	55.6	0.3
5	940	0.581	14.022	2.0250E-03	7.1950E-01	1.2690E-02	3.8990E+00	1.9250E+03	55.3	0.3
6	990	0.690	26.941	4.3140E-03	1.0170E+00	1.3840E-02	4.4670E+00	1.0350E+03	53.9	0.3
7	1040	0.765	39.208	7.6360E-03	1.4490E+00	1.5130E-02	5.4960E+00	7.1980E+02	55.3	0.3
8	1080	0.841	48.512	1.0800E-02	2.3420E+00	1.6040E-02	6.2330E+00	5.7710E+02	53.2	0.4
9	1120	0.907	46.979	1.0430E-02	2.4230E+00	1.5860E-02	6.1880E+00	5.9340E+02	54.3	0.4
10	1180	0.953	49.036	1.1210E-02	3.0650E+00	1.6330E-02	6.3030E+00	5.6200E+02	53.2	0.4
11	1240	0.984	74.449	3.2300E-02	6.0900E+00	2.0690E-02	1.2220E+01	3.7820E+02	52.0	0.7
12	1300	0.992	66.567	2.4350E-02	6.8230E+00	1.9210E-02	1.0050E+01	4.1250E+02	55.9	1.7
13	1400	0.997	77.689	4.1850E-02	9.6680E+00	2.1570E-02	1.4990E+01	3.5810E+02	55.8	1.5
14	1500	1.000	86.373	7.5370E-02	3.7690E+00	2.6250E-02	2.5480E+01	3.3800E+02	57.7	3.4

04YJ-3, sample mass = 4.3 mg, plateau age = 54.9 ± 0.3 Ma (steps 3–13), J-value = 0.00934382.

Table 5: Whole-rock Ar–Ar dating of the Palaeocene Yanji adakitic andesites by the laser method

Step	Output laser power (W)	³⁶ Ar (a)	³⁷ Ar (ca)	³⁸ Ar (cl)	³⁹ Ar (k)	⁴⁰ Ar (r)	Age (Ma)	±2σ (Ma)	⁴⁰ Ar (r)	³⁹ Ar (k) (%)	K/Ca (%)	±2σ
<i>Sample 05YJ-64</i>												
1	1.48	0.4290	2.9414	0.0037	2.0231	6.9195	72.36	24.4	5.2	0.94	0.385	0.023
2	1.99	0.3835	4.1530	0.0000	4.6469	12.9173	59.03	10.9	10.2	2.16	0.627	0.036
3	2.57	0.2881	4.9666	0.0000	6.9808	19.2729	58.63	5.6	18.5	3.25	0.787	0.045
4	3.14	0.3116	6.6529	0.0000	9.7367	26.8792	58.63	4.2	22.6	4.53	0.820	0.047
5	3.85	0.3228	9.9860	0.0000	13.6458	37.6029	58.52	2.9	28.3	6.35	0.765	0.043
6	4.41	0.2742	11.4670	0.0000	13.7879	37.7342	58.13	2.7	31.8	6.41	0.673	0.038
7	5.03	0.3012	18.8954	0.0034	18.6863	51.4214	58.44	2.1	36.6	8.69	0.554	0.031
8	5.58	0.2380	19.7990	0.0037	17.6551	48.8042	58.70	1.9	40.9	8.21	0.499	0.028
9	6.12	0.1854	18.5620	0.0054	14.6301	40.4048	58.65	2.0	42.4	6.80	0.441	0.025
10	6.72	0.2003	24.0065	0.0142	16.8645	46.8412	58.98	1.8	44.1	7.84	0.393	0.022
11	7.71	0.2425	35.5336	0.0208	20.8990	57.6861	58.62	1.7	44.6	9.72	0.329	0.018
12	8.99	0.2563	56.8157	0.0299	24.2738	66.7673	58.42	1.6	46.8	11.29	0.239	0.013
13	10.55	0.2422	50.0441	0.0204	22.9870	63.1361	58.33	1.5	46.8	10.69	0.257	0.014
14	12.33	0.2788	58.8666	0.0355	28.1913	77.2940	58.23	1.4	48.4	13.11	0.268	0.015
<i>Sample 05YJ-20</i>												
1	1.11	0.0939	1.9880	0.0000	3.2843	8.1150	52.48	11.6	22.6	0.85	0.925	0.055
2	1.70	0.1410	4.9839	0.0000	11.5075	31.6569	58.34	3.6	43.1	2.97	1.293	0.073
3	2.21	0.1459	7.0448	0.0000	17.7792	48.9899	58.43	2.4	53.1	4.58	1.413	0.079
4	2.71	0.1565	8.8414	0.0000	22.0258	59.4544	57.26	2.0	56.2	5.68	1.395	0.078
5	3.28	0.1654	10.6158	0.0000	24.0955	65.5765	57.72	1.8	57.2	6.21	1.271	0.070
6	3.85	0.2006	15.0721	0.0000	29.7172	80.9090	57.75	1.6	57.6	7.66	1.104	0.061

(continued)

Table 5: Continued

Step	Output laser power (W)	³⁶ Ar (a)	³⁷ Ar (ca)	³⁸ Ar (cl)	³⁹ Ar (k)	⁴⁰ Ar (r)	Age	±2σ (Ma)	⁴⁰ Ar (r)	³⁹ Ar (k) (%)	K/Ca (%)	±2σ
7	4-43	0.1725	15.4944	0.0000	27.7343	75.0354	57.39	1.6	59.5	7.15	1.002	0.055
8	4-96	0.1555	17.5437	0.0056	27.3822	73.8424	57.21	1.6	61.6	7.06	0.874	0.048
9	5-51	0.1595	20.4581	0.0116	27.2806	73.7294	57.33	1.6	60.9	7.03	0.747	0.041
10	6-05	0.1223	18.1125	0.0118	23.8133	64.7148	57.64	1.8	64.1	6.14	0.736	0.041
11	6-72	0.0995	18.0175	0.0126	21.0310	57.0143	57.50	2.0	65.9	5.42	0.654	0.036
12	7-71	0.1081	29.6276	0.0208	22.8281	61.4392	57.10	1.8	65.7	5.88	0.431	0.024
13	8-68	0.1074	25.8884	0.0190	21.9045	58.8546	57.00	1.9	64.9	5.64	0.474	0.026
14	10-55	0.1582	46.1346	0.0396	32.4337	87.2328	57.06	1.4	65.0	8.36	0.394	0.022
15	12-33	0.1845	41.8364	0.0333	36.8810	98.8004	56.83	1.3	64.3	9.50	0.494	0.027
16	15-47	0.1913	62.3240	0.0516	38.3707	101.3709	56.06	1.1	64.1	9.89	0.345	0.019
<i>Sample 05YJ-1</i>												
1	1-48	0.4304	4.0827	0.0258	8.9140	38.9179	91.70	4.9	23.4	2.52	1.223	0.067
2	1-84	0.2306	4.7728	0.0036	12.2609	39.3946	67.93	2.3	36.6	3.46	1.439	0.079
3	2-21	0.1593	5.3423	0.0000	14.1307	39.9455	59.90	2.2	45.9	3.99	1.481	0.083
4	2-57	0.1902	7.6754	0.0000	17.9932	50.2076	59.14	1.9	47.1	5.08	1.313	0.073
5	3-07	0.1573	12.9082	0.0000	24.6090	66.2449	57.09	1.2	58.7	6.94	1.068	0.059
6	3-64	0.1519	17.0313	0.0000	27.7835	73.7929	56.34	1.3	62.1	7.84	0.914	0.051
7	4-13	0.0942	13.5372	0.0000	22.4304	59.7748	56.52	1.3	68.1	6.33	0.928	0.051
8	4-69	0.1435	32.0273	0.0015	39.5624	105.0130	56.30	1.0	71.1	11.16	0.692	0.038
9	5-37	0.0922	30.6275	0.0006	34.5854	91.6926	56.24	1.1	77.0	9.76	0.632	0.035
10	5-85	0.0904	36.8606	0.0080	35.1497	94.0543	56.75	0.8	77.7	9.92	0.534	0.029
11	6-39	0.0549	34.9810	0.0190	26.6408	71.2533	56.73	0.7	81.3	7.52	0.426	0.023
12	7-05	0.0434	32.4408	0.0186	21.1520	55.9875	56.15	0.8	81.2	5.97	0.365	0.020
13	7-90	0.0467	42.8364	0.0291	21.5698	56.8550	55.92	0.8	80.3	6.09	0.282	0.015
14	8-99	0.0224	20.5730	0.0125	10.3717	27.3051	55.85	1.4	80.3	2.93	0.282	0.015
15	10-55	0.0466	41.0039	0.0271	18.1117	47.6083	55.77	0.9	77.4	5.11	0.247	0.014
16	12-33	0.0298	29.7508	0.0220	12.8919	33.7487	55.54	1.3	79.2	3.64	0.243	0.013
17	15-47	0.0192	19.6788	0.0110	6.1945	16.1101	55.18	2.3	73.8	1.75	0.176	0.010

a, air; ca, calcium; cl, chlorine; k, potassium; r, radiogenic; ³⁶Ar, ³⁷Ar, ³⁸Ar, ³⁹Ar and ⁴⁰Ar are measured intensities of the respective isotopes. Sample 05YJ-64, plateau age = 58.5 ± 0.6 Ma (steps 1–14), J-value = 0.011965. Sample 05YJ-20, plateau age = 57.2 ± 0.5 Ma (steps 1–16), J-value = 0.011947. Sample 05YJ-1, plateau age = 56.3 ± 0.3 Ma (steps 4–17), J-value = 0.011943.

magma is required (e.g. Green, 1982). Possible ways to increase the magma temperature are by addition of another high-*T* magma, by hybridization with hot mantle or by rapid decompressive crystallization.

Melt–mantle interaction?

Melt–mantle interaction might be an alternative way of creating the compositional zonations observed in clinopyroxene. Such a model has been widely applied to interpret the high Mg-number, and high Cr and Ni contents, in most of the modern adakites occurring at convergent plate margins and in experimental slab melts hybridized by mantle peridotite (Kay, 1978; Yogodzinski *et al.*, 1995; Rapp *et al.*, 1999; Tsuchiya *et al.*, 2005; Guo *et al.*, 2006;

Xiong *et al.*, 2006). Decomposition of olivine and possibly orthopyroxene in mantle peridotite lead to an increase of MgO, Cr and Ni in the hybridized slab melts, and thus can result in reverse zonations in crystallizing minerals. If such a petrogenetic process was the case for the Yanji adakitic andesites, the high-Fe clinopyroxene cores would reflect crystallization from the slab melt (before assimilation of peridotite), whereas the high Mg-number clinopyroxene rims would reflect interaction between that melt and the surrounding mantle peridotite.

In general, high-pressure slab melts (e.g. adakites), derived from eclogitic protoliths with residual pyroxene, garnet, amphibole and rutile are characterized by high Sr, low Y and HREE (Defant & Drummond, 1990;

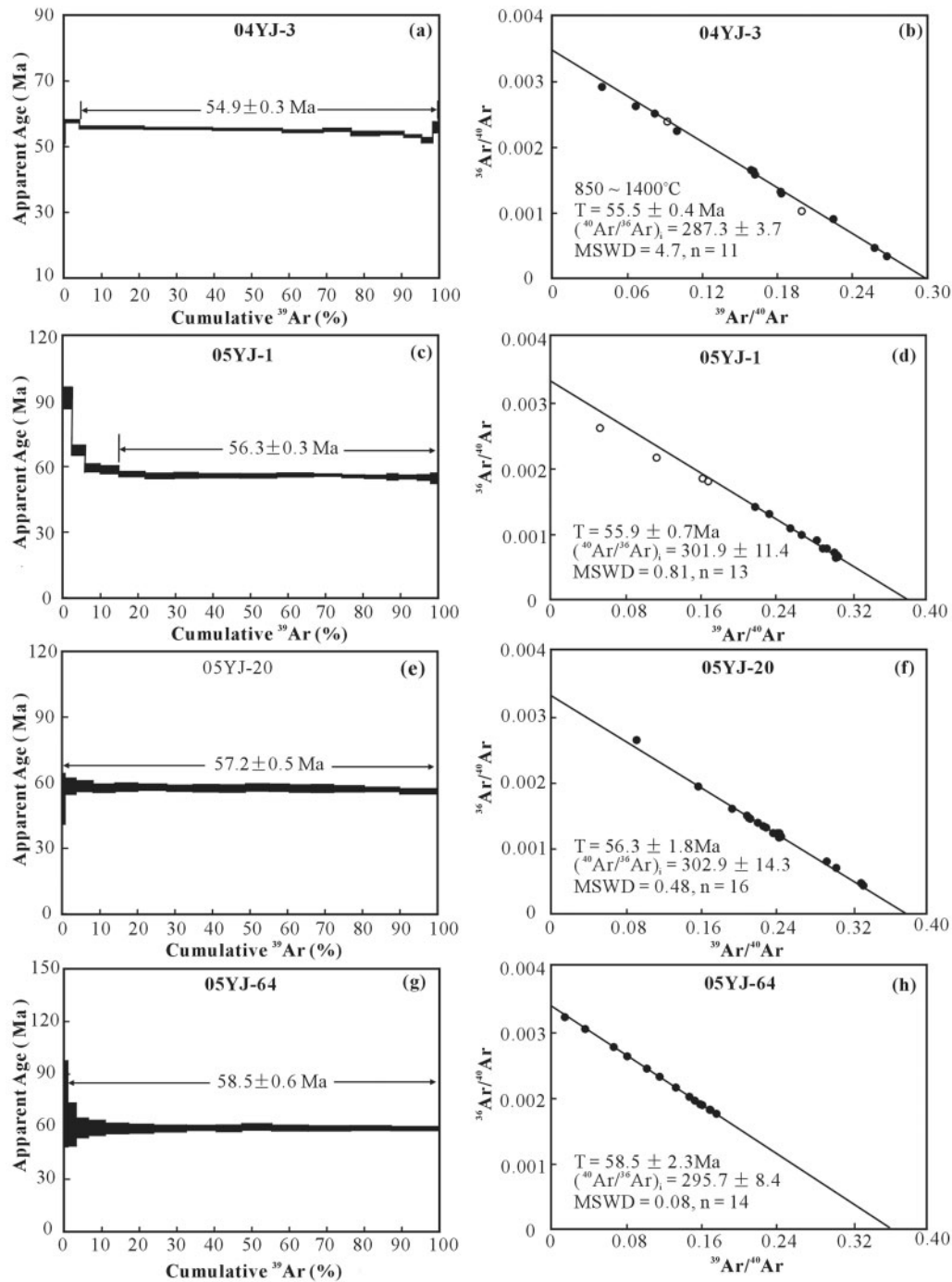


Fig. 8. Ar–Ar dating results for the Yanji adakitic andesites.

Smithies, 2000; Martin *et al.*, 2005). During the ascent of these melts, clinopyroxene crystallizes without significant coexisting plagioclase. However, the Fe-rich clinopyroxene cores in the Yanji adakitic andesites show large negative Eu anomalies combined with low Sr and $\text{Nd}/\text{Yb}_{\text{CN}}$ (Figs 6 and 7). These compositional features suggest crystallization accompanied by plagioclase—a paragenesis

very unlike that of an ascending adakitic slab melt. In addition, if the high Mg-number clinopyroxene rims formed by melt–peridotite interaction, they should have lower incompatible element (e.g. Sr) concentrations than those of the Fe-rich cores, as the mantle wedge should have much lower incompatible element concentrations than a slab melt. Experimental results show

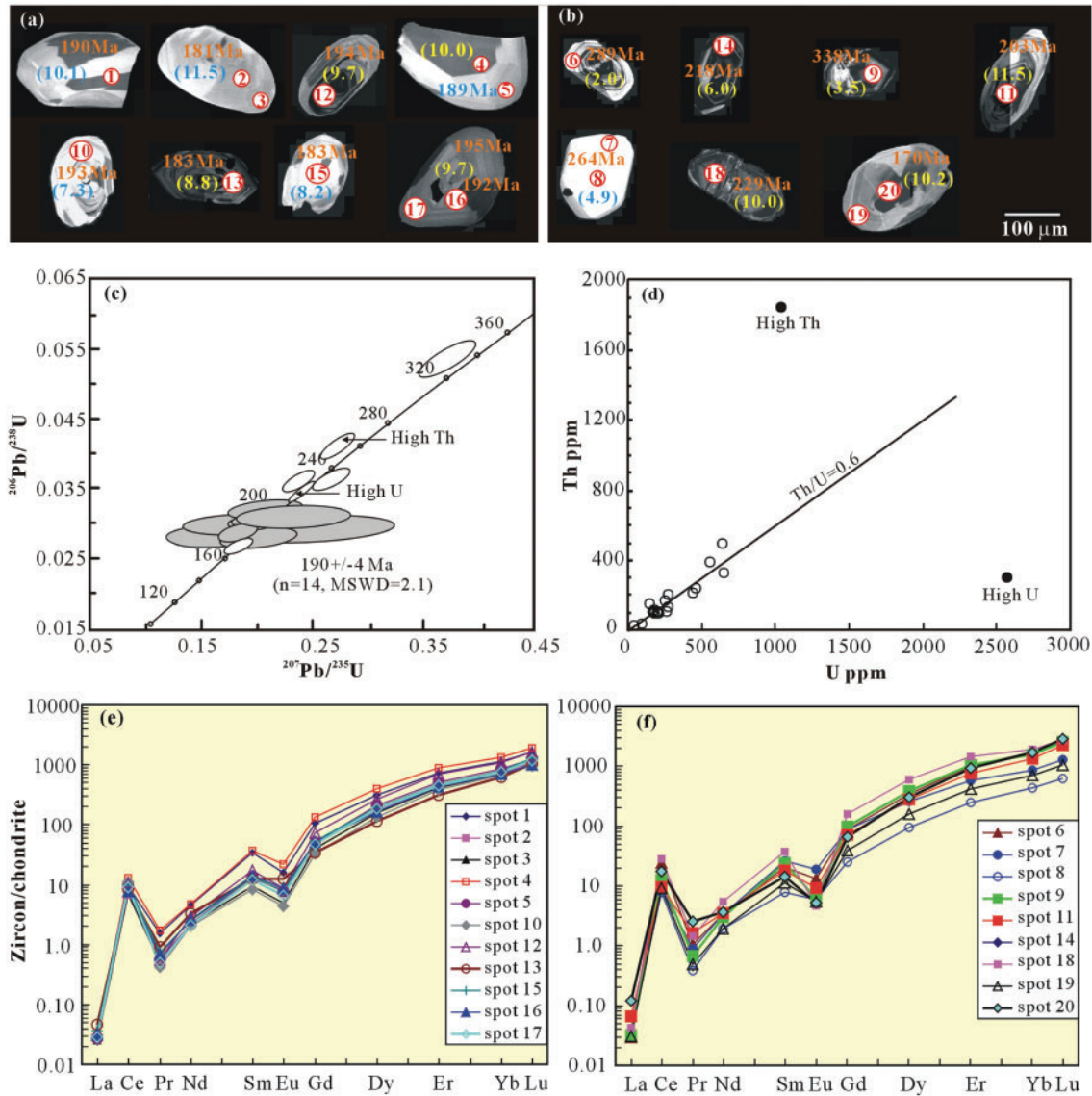


Fig. 9. Representative cathodoluminescence (CL) images (a and b), U–Pb dating results (c and d) and chondrite-normalized REE patterns (e and f) for zircons from sample 04YJ-6. In (a) and (b), apparent $^{206}\text{Pb}/^{238}\text{U}$ ages, ϵ_{Hf} and analytical spot number by IMS-5f.

that mantle hybridization does not notably increase the incompatible element compositions of hybridized melts (Rapp *et al.*, 1999).

Accordingly, although a melt–mantle interaction model could explain the observed major element variations in the clinopyroxene phenocrysts in the Yanji adakitic andesites, it is highly unlikely that it could account for their trace element characteristics. Furthermore, it appears unlikely that the Fe-rich clinopyroxene cores crystallized from an adakitic slab melt.

Magma mixing?

Our ion microprobe data for clinopyroxene are similar to those presented by Yögodzinski & Kelemen (1998),

who showed that clinopyroxene in some ‘primitive’ adakites from the Aleutian Arc had low Mg-number cores with lower Sr and Nd/Yb than the high Mg-number rims. To explain these features, they proposed mixing between a primitive adakite with high Mg-number, Sr and Nd/Yb, and an evolved arc-basalt or basaltic andesite with relatively low Mg-number, Sr and Nd/Yb (Yögodzinski & Kelemen, 1998).

High Mg-number clinopyroxene phenocrysts in the primitive Aleutian adakites contain inclusions of hypersthene, which probably crystallized from an evolved arc basalt or basaltic andesite. Clinopyroxene phenocrysts in the Yanji adakitic andesites contain inclusions of bronzite and low-An plagioclase. Bronzite is a common

Table 6: SHRIMP U–Pb dating of zircons in sample 04YJ-6

Spot	U (ppm)	Th (ppm)	²³² Th/ ²³⁸ U	²⁰⁶ Pb* (ppm)	²⁰⁶ Pb/ ²³⁸ U	±%	²⁰⁷ Pb/ ²³⁵ U	±%	²⁰⁶ Pb/ ²³⁸ U age (Ma)	±2σ
1	152	149	1.0111	3.67	0.0276	2.2	0.163	14.0	177	3.8
2	643	493	0.7930	20.0	0.0362	1.8	0.254	2.9	229	4.2
3	1039	1846	1.8353	37.0	0.0413	1.8	0.289	2.7	261	4.7
4	463	242	0.5398	21.6	0.0541	2.0	0.420	3.0	338	6.8
5	199	108	0.5615	5.20	0.0293	2.4	0.116	36.0	191	3.9
6	275	205	0.7688	7.23	0.0302	2.0	0.237	12.0	190	4.0
7	198	94	0.4924	5.28	0.0305	2.1	0.218	10.0	193	4.0
8	444	209	0.4872	12.3	0.0318	2.0	0.192	12.0	203	3.9
9	2567	305	0.1228	76.2	0.0344	1.8	0.236	2.2	218	3.9
10	210	101	0.4995	5.62	0.0305	2.2	0.198	13.0	194	4.1
11	259	104	0.4145	6.48	0.0288	2.1	0.188	7.2	183	3.7
12	648	324	0.5166	15.1	0.0268	1.9	0.192	4.4	170	3.2
13	560	388	0.7159	17.6	0.0362	1.9	0.245	4.9	229	4.2
14	181	113	0.6446	4.79	0.0303	2.5	0.213	9.1	192	4.7
15	182	95	0.5403	4.95	0.0304	2.3	0.176	20.0	195	4.0
16	170	107	0.6489	4.67	0.0308	2.3	0.220	16.0	195	4.2
17	41.3	25.8	0.6455	1.73	0.0429	5.1	0.420	46.0	264	11
18	180	101	0.5801	4.82	0.0300	3.0	0.339	15.0	183	5.3
19	272	137	0.5191	7.17	0.0297	2.7	0.198	21.0	189	4.9
20	98.6	39.8	0.4168	2.51	0.0280	3.1	0.135	37.0	181	5.0
21	253	172	0.7056	6.63	0.0301	2.6	0.230	9.3	190	4.9

²⁰⁶Pb* is the concentration of radiogenic ²⁰⁶Pb. ²⁰⁶Pb/²³⁸U age is corrected for common Pb, by assuming ²⁰⁶Pb/²³⁸U–²⁰⁷Pb/²³⁵U age-concordance.

Table 7: Trace element compositions of zircons in sample 04YJ-6

Spot	Age (Ma)	U	Th	Y	La	Ce	Pr	Nd	Sm	Eu	Gd	Dy	Er	Yb	Lu	Hf	Eu/Eu*
1	190	275	205	978	0.006	5.85	0.14	2.08	4.98	0.89	21.05	78.03	118	184	40.0	4295	0.11
2	181 (c)	98.6	39.8	536	0.006	4.22	0.06	0.95	1.87	0.48	9.85	43.00	70.5	119	26.7	4057	0.14
3	181 (r)	98.6	39.8	490	0.006	4.42	0.05	0.99	1.40	0.28	7.98	38.98	66.3	113	25.2	4211	0.10
4	189 (c)	272	137	1122	0.007	7.85	0.16	2.21	5.57	1.22	26.64	99.58	144	214	47.8	4331	0.13
5	189 (r)	272	137	670	0.007	6.08	0.05	1.01	2.03	0.44	10.28	51.14	82.0	137	30.6	4330	0.12
6	261	1039	1846	1158	0.007	14.92	0.10	1.54	3.02	0.74	17.23	84.75	160	273	67.2	3977	0.12
7	264 (r)	41.3	25.8	700	0.008	5.64	0.08	1.57	3.85	1.08	17.74	63.57	90.7	140	31.2	3956	0.17
8	264 (c)	41.3	25.8	313	0.008	4.88	0.04	0.87	1.15	0.34	4.96	23.28	39.6	70.2	15.3	3942	0.18
9	338	463	242	1229	0.008	7.74	0.06	1.36	3.55	0.35	19.83	95.65	168	253	62.2	3423	0.05
10	193	198	94	455	0.007	6.82	0.04	0.92	1.22	0.25	6.49	33.53	60.4	108	23.9	4632	0.11
11	203	444	209	923	0.016	5.91	0.15	1.59	2.72	0.52	14.02	68.36	123	214	56.6	4171	0.10
12	194	210	101	882	0.008	6.57	0.05	1.36	2.54	0.49	14.45	65.95	111	173	40.3	4393	0.10
13	183	259	104	471	0.011	5.09	0.09	1.51	1.83	0.70	6.84	28.63	50.4	98.9	25.9	3792	0.27
14	218	2567	305	1298	0.029	10.70	0.23	1.66	2.14	0.30	12.91	75.09	153	272	71.2	4524	0.07
15	183	259	104	611	0.009	5.96	0.07	1.16	2.03	0.43	10.70	46.58	76.1	129	31.0	3940	0.11
16	192	181	113	543	0.007	4.71	0.06	1.19	2.09	0.50	10.19	40.74	68.5	112	25.3	3916	0.14
17	195	170	107	599	0.007	5.50	0.05	0.96	1.77	0.36	9.36	45.37	73.2	124	28.8	4106	0.11
18	229	643	493	1777	0.010	17.27	0.13	2.54	5.66	0.26	31.61	146.71	231	305	67.3	2688	0.02
19	170 (r)	648	324	523	0.007	5.64	0.05	0.89	1.70	0.31	7.90	39.00	66.5	113	26.1	4184	0.11
20	170 (c)	648	324	818	0.008	5.29	0.06	1.12	2.10	0.53	11.25	56.14	106	184	47.0	3566	0.13

Age and U and Th contents were determined by SHRIMP; other elements were analyzed by Cameca IMS-5f; r and c respectively represent rim and core of a single zircon grain. $E_u/E_u^* = E_{uCN}/(S_{mCN} * G_{dCN})^{0.5}$.

Table 8: Major and trace element compositions of the Palaeocene Yanji adakitic andesites

Sample:	04YJ-1	04YJ-2	04YJ-3	04YJ-4	04YJ-5	04YJ-6	04YJ-7	04YJ-8	04YJ-9	05YJ-1	05YJ-3	05YJ-6	05YJ-7
SiO ₂	61.43	61.54	60.92	61.63	61.93	61.77	61.25	61.74	62.20	61.59	61.32	61.48	61.38
TiO ₂	0.87	0.87	0.86	0.85	0.86	0.87	0.88	0.86	0.86	0.87	0.87	0.88	0.87
Al ₂ O ₃	15.63	15.61	15.48	15.45	15.67	15.65	15.59	15.61	15.54	15.48	15.48	15.65	15.68
Fe ₂ O ₃	4.14	3.98	4.03	4.11	4.07	4.11	4.17	4.37	4.10	3.72	3.64	3.80	3.64
MnO	0.07	0.07	0.07	0.07	0.08	0.07	0.07	0.08	0.08	0.07	0.07	0.06	0.07
MgO	4.14	4.24	4.06	4.02	4.17	4.05	4.05	4.14	4.06	4.36	4.24	4.08	4.11
CaO	6.90	7.07	7.04	6.84	7.06	7.07	6.85	7.00	6.77	7.35	7.29	7.16	7.24
Na ₂ O	3.49	3.50	3.50	3.48	3.52	3.47	3.46	3.47	3.58	3.26	3.29	3.26	3.20
K ₂ O	1.78	1.78	2.02	1.78	1.78	1.76	1.81	1.78	1.84	1.69	1.70	1.78	1.82
P ₂ O ₅	0.24	0.26	0.27	0.25	0.25	0.25	0.25	0.21	0.25	0.27	0.26	0.26	0.28
LOI	1.27	1.17	2.34	1.22	1.24	1.13	1.55	1.32	1.21	1.13	1.23	1.30	1.22
Total	99.94	100.10	100.59	99.70	100.63	100.21	99.94	100.59	100.49	99.78	99.41	99.70	99.48
Mg-no.	66.7	68.1	66.9	66.2	67.2	66.3	66.1	65.5	66.4	70.1	70.0	68.2	69.3
A/CNK	0.77	0.76	0.75	0.77	0.76	0.76	0.77	0.77	0.77	0.75	0.75	0.77	0.77
Sc	8.8	9.4	8.7	9.2	9.1	9.3	9.1	9.0	8.8	9.0	9.2	8.3	8.2
V	72	77	71	72	75	77	75	73	72	75	74	73	70
Cr	134	149	135	145	142	161	146	154	141	149	145	142	128
Co	14.3	14.9	14.0	14.8	15.0	15.0	14.4	14.6	14.4	16.3	16.9	16.6	15.0
Ni	104	114	101	109	106	113	112	117	107	93	98	105	86
Rb	16.1	16.0	14.4	16.2	15.0	14.6	15.2	15.9	18.0	13.4	14.9	15.6	15.0
Sr	2148	2282	2253	2243	2276	2241	2209	2277	2252	2024	2171	2061	2013
Y	10.6	11.0	10.7	11.0	11.0	10.8	11.0	10.4	11.0	10.0	10.8	10.5	10.4
Zr	155	157	150	157	156	155	158	158	155	146	150	147	141
Nb	5.3	5.5	5.1	5.4	5.4	5.3	5.4	5.3	5.3	4.5	4.7	4.7	4.6
Ba	520	477.1	494	496.9	497.8	484.2	496.4	493.1	487.8	428.3	443.4	446.7	500.4
La	43.05	44.33	45.93	44.00	43.90	44.36	44.64	42.40	44.32	41.30	42.60	39.72	43.05
Ce	94.04	97.92	99.98	99.11	97.73	98.17	97.53	92.92	96.66	92.11	92.39	88.72	95.23
Pr	11.56	12.00	12.36	12.03	11.98	11.72	11.95	11.48	11.94	11.42	11.24	11.12	12.15
Nd	42.12	44.25	44.90	43.38	44.53	43.31	44.28	41.72	44.40	41.30	42.43	43.09	44.81
Sm	6.23	6.49	6.68	6.61	6.78	6.50	6.54	6.33	6.57	5.53	5.81	6.11	6.29
Eu	1.63	1.74	1.75	1.74	1.76	1.73	1.75	1.74	1.70	1.47	1.51	1.74	1.72
Gd	3.46	3.71	3.88	3.66	3.77	3.67	3.85	3.50	3.62	3.67	3.78	4.13	4.06
Tb	0.48	0.52	0.51	0.52	0.49	0.50	0.52	0.50	0.50	0.41	0.45	0.47	0.47
Dy	2.33	2.46	2.40	2.39	2.38	2.37	2.45	2.27	2.39	1.94	1.99	2.28	2.24
Ho	0.40	0.43	0.41	0.42	0.42	0.43	0.43	0.40	0.41	0.34	0.36	0.39	0.38
Er	1.12	1.10	1.08	1.05	1.09	1.08	1.07	1.02	1.03	0.90	1.00	1.07	1.03
Tm	0.15	0.15	0.14	0.15	0.15	0.15	0.15	0.14	0.15	0.12	0.14	0.15	0.14
Yb	0.94	1.01	0.89	0.97	0.96	0.95	0.96	0.90	0.95	0.79	0.87	0.90	0.89
Lu	0.14	0.15	0.14	0.15	0.15	0.15	0.16	0.14	0.14	0.12	0.14	0.13	0.13
Hf	4.13	4.18	4.00	4.14	4.10	4.14	4.27	4.21	4.15	3.43	4.02	3.81	3.64
Ta	0.33	0.32	0.30	0.32	0.31	0.30	0.32	0.31	0.32	0.28	0.31	0.30	0.31
Pb	6.21	5.91	6.00	9.16	8.71	8.36	6.46	8.19	8.58	5.73	5.56	8.28	6.88
Th	8.00	8.01	8.19	8.25	8.39	7.82	8.06	8.09	10.43	6.79	7.02	7.19	7.62
U	0.81	0.86	0.75	0.84	0.80	0.75	0.75	0.81	0.79	0.69	0.73	0.75	0.77

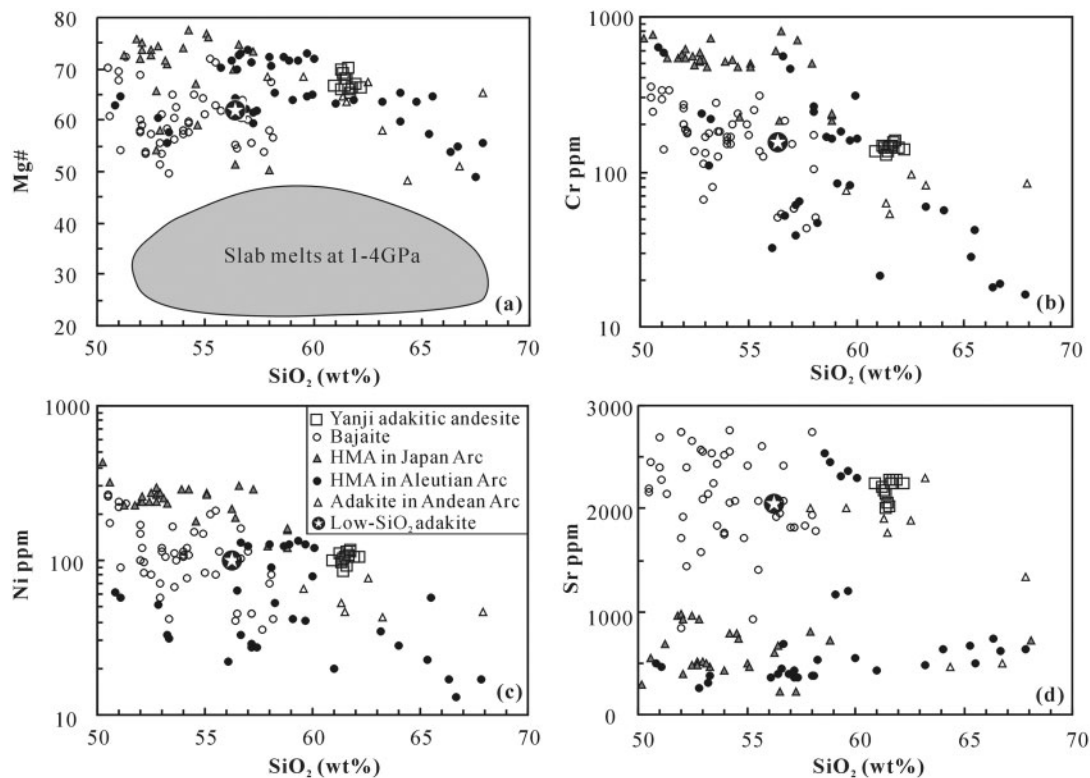


Fig. 10. SiO_2 vs Mg-number (a), Cr (b), Ni (c) and Sr (d) for the Yanji adakitic andesites. Comparison data are high-Mg andesites (HMA) from the Japan, Andean and Aleutian Arcs and bajaites from Baja California. Data sources: HMAs in the Japan Arc from Shimoda *et al.* (1998), Tatsumi *et al.* (2003) and Kamei *et al.* (2004); HMAs in the Aleutian Arc from Yögodzinski *et al.* (1995); adakites from the Andean Arc from Kay *et al.* (1993) and Stern & Kilian (1996); bajaites from Baja California from Calmus *et al.* (2003); low- SiO_2 adakite from Martin *et al.* (2005).

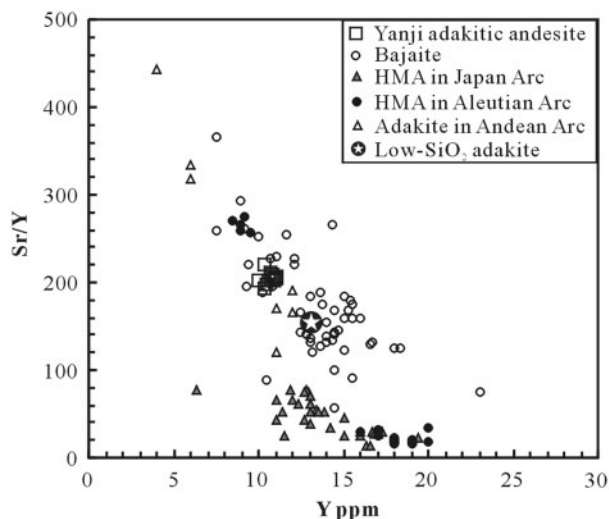


Fig. 11. Y vs Sr/Y variation in the Yanji adakitic andesites. Comparison data sources are the same as in Fig. 10.

early-crystallizing phase in high Mg-number sanukitoid magmas interpreted to be melts of a peridotite previously metasomatized via addition of slab melt (Shirey & Hanson, 1984; Tatsumi, 2006). In these cases, both the

residual bronzite and the high Mg-number clinopyroxene are likely to be fractionating phases in the high Mg-number primitive magma. It is possible that the clinopyroxene phenocrysts and bronzite inclusions in the Yanji adakitic andesites can be interpreted in the same way.

In contrast, the low An content of the plagioclase inclusions in the Yanji clinopyroxene phenocrysts implies a more felsic magmatic source, possibly more consistent with the high-Fe compositions of some clinopyroxene cores, as both Fe-rich clinopyroxene and plagioclase with an An content range of 35–41 are common fractionating phases in andesitic–dacitic melts. Experimental results show that low-An plagioclase is unstable at high temperatures (e.g. within the hot mantle wedge), and so the low-An plagioclase inclusions hosted in clinopyroxene phenocrysts argue further against an origin from a felsic slab melt—mantled by high Mg-number clinopyroxene (e.g. Green, 1982). We suggest that the low-An plagioclase and the Fe-rich clinopyroxene (cores) coexisted as early fractionating phases in a felsic magma—but not a slab melt.

Further, compared with the Fe-rich clinopyroxene cores, the high Mg-number clinopyroxenes generally have higher Sr, Sr/Y and $\text{Nd}/\text{Yb}_{\text{CN}}$, and negligible Eu anomalies,

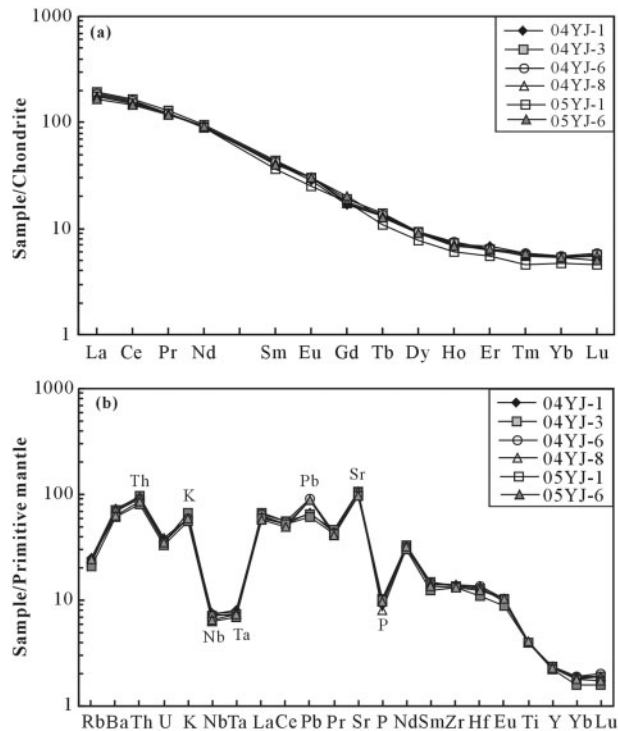


Fig. 12. Chondrite-normalized REE patterns (a) and primitive mantle-normalized trace element patterns (b) of the Yanji adakitic andesites. Trace element concentrations for both chondrites and primitive mantle are from Sun & McDonough (1989).

and so are unlikely to have coexisted with plagioclase during crystal growth. This is consistent with petrographic observations that no plagioclase phenocrysts have been found.

We envisage that the clinopyroxene and plagioclase compositional relationships and zoning patterns developed in a high Mg-number adakitic magma that ascended from the mantle and mixed with a felsic lower crustal melt that was already crystallizing Fe-rich clinopyroxene and low-An plagioclase.

Constraints on the possible magma mixing components

The above discussion, based on mineralogical evidence from clinopyroxene phenocrysts and microcrystalline plagioclase, strongly suggests that magma mixing influenced the evolution of the Yanji adakitic andesites. In the following section, we discuss the possible magma components involved in this mixing process.

The felsic magma

This magma might be either a differentiate of a mantle-derived basalt or a crust-derived melt. As illustrated in Fig. 7, the felsic magmatic component is characterized by low MgO and Sr but high Y and HREE contents,

very different from adakites occurring in modern subduction zones (e.g. Defant & Drummond, 1990; Martin *et al.*, 2005). In the Yanji area and in the adjacent regions, the lack of basaltic magmas contemporaneous with the Palaeocene adakitic andesites suggests that the felsic magma component was derived from the local crust (e.g. Liu *et al.*, 2001).

Using experimental REE partition coefficients for clinopyroxene in basaltic–andesitic, andesitic–dacitic and low-Si and high-Si rhyolitic melts, respectively (e.g. Luhr & Carmichael, 1980; Dostal *et al.*, 1983; Nash & Crecraft, 1985; Sisson, 1991), we have recalculated the possible REE contents of the melts in equilibrium with the Fe-rich clinopyroxene cores and high Mg-number clinopyroxene, respectively. From these calculations, it becomes obvious that mixing between a rhyolitic melt (whether low-Si or high-Si in composition) coexisting with the Fe-rich clinopyroxene cores and a mantle-derived high Mg-number magma coexisting with the high Mg-number clinopyroxene could not have produced the whole-rock REE contents of the Yanji adakitic andesites. However, the whole-rock REE contents in these rocks can be successfully modelled by mixing between an andesitic–dacitic melt coexisting with the Fe-rich clinopyroxene cores and a mantle-derived high Mg-number magma (Fig. 15; see also Table 11).

The high Y concentrations and weakly fractionated REE patterns in the Fe-rich clinopyroxene cores point to protoliths with little or no residual garnet. In contrast, Sr is compatible in plagioclase, and therefore low Sr in Fe-rich clinopyroxene might be attributed either to low Sr concentration in the magma in equilibrium with residual plagioclase or to plagioclase fractionation during clinopyroxene crystallization. Therefore, we can summarize the characteristics of the felsic magma component as follows: (1) it was andesitic–dacitic in composition with high Y and a significant negative Eu anomaly; (2) the melt was in equilibrium with plagioclase (either as a fractionating phase in the melt or as a residual phase during melting) but not with garnet, arguing against an eclogitic protolith.

The high Mg-number melt

The other mixing component must have low SiO₂, Y and HREE, and high MgO (or Mg-number), Sr and Sr/Y ratios, analogous to a high Mg-number adakite (e.g. Yogodzinski *et al.*, 1995; Martin *et al.* 2005). Mass balance considerations suggest that such high Mg-number adakites could not be derived from melting of an eclogite-facies basaltic lower crust (Petford & Atherton, 1996; Yogodzinski & Kelemen, 1998). As discussed above, slab melt–mantle interaction cannot account for the trace element characteristics of the clinopyroxene phenocrysts. Therefore, we suggest that the high Mg-number melt was

Table 9: Sr–Nd–Pb isotopic compositions of the Palaeocene Yanji adakitic andesites

Sample	Rb (ppm)	Sr (ppm)	Sm (ppm)	Nd (ppm)	U (ppm)	Th (ppm)	Pb (ppm)	⁸⁷ Rb/ ⁸⁶ Sr	⁸⁷ Sr/ ⁸⁶ Sr ± 2σ	⁸⁷ Sr/ ⁸⁶ Sr(i)	¹⁴⁷ Sm/ ¹⁴⁴ Nd	¹⁴³ Nd/ ¹⁴⁴ Nd ± 2σ	ε _{Nd} (t)	T _{DM} (Ma)
04YJ-1	16.05	2148	6.233	42.12	0.806	8.001	6.211	0.0209	0.703147 ± 8	0.70313	0.0910	0.512882 ± 9	5.51	334
04YJ-2	15.98	2282	6.49	44.25	0.86	8.007	5.907	0.0196	0.703071 ± 11	0.70306	0.0902	0.512920 ± 8	6.26	284
04YJ-4	16.23	2243	6.605	43.38	0.842	8.246	9.157	0.0202	0.703163 ± 21	0.70315	0.0936	0.512877 ± 9	5.38	348
04YJ-5	15.01	2276	6.777	44.53	0.802	8.386	8.711	0.0184	0.703173 ± 14	0.70316	0.0936	0.512898 ± 8	5.80	320
04YJ-6	14.55	2241	6.499	43.31	0.752	7.822	8.36	0.0181	0.702993 ± 14	0.70298	0.0923	0.512823 ± 7	4.34	412
04YJ-7	15.23	2209	6.54	44.28	0.748	8.062	6.455	0.0192	0.703113 ± 13	0.70310	0.0908	0.512795 ± 8	3.81	442
04YJ-9	18.04	2252	6.565	44.4	0.793	10.43	8.577	0.0224	0.703111 ± 15	0.70309	0.0909	0.512795 ± 7	3.81	442

Sample:	²⁰⁶ Pb/ ²⁰⁴ Pb ± 2σ	²⁰⁷ Pb/ ²⁰⁴ Pb ± 2σ	²⁰⁸ Pb/ ²⁰⁴ Pb ± 2σ	²³⁸ U/ ²⁰⁴ Pb	²³⁵ U/ ²⁰⁴ Pb	²³² Th/ ²⁰⁴ Pb	²⁰⁶ Pb/ ²⁰⁴ Pb(i)	²⁰⁷ Pb/ ²⁰⁴ Pb(i)	²⁰⁸ Pb/ ²⁰⁴ Pb(i)
04YJ-1	18.062 ± 10	15.498 ± 10	38.095 ± 11	7.46	0.05	76.54	18 055	15 547	37 886
04YJ-2	18.020 ± 7	15.453 ± 7	37.925 ± 7	8.37	0.06	80.53	18 012	15 508	37 706
04YJ-4									
04YJ-5	17.988 ± 10	15.453 ± 13	37.908 ± 16	5.29	0.04	57.20	17 984	15 488	37 753
04YJ-6	17.997 ± 6	15.470 ± 6	37.948 ± 6	5.17	0.04	55.59	17 993	15 504	37 796
04YJ-7	18.014 ± 9	15.474 ± 8	38.007 ± 9	6.66	0.05	74.20	18 008	15 517	37 805
04YJ-9	17.998 ± 7	15.460 ± 7	37.928 ± 6	5.32	0.04	72.25	17 993	15 495	37 731

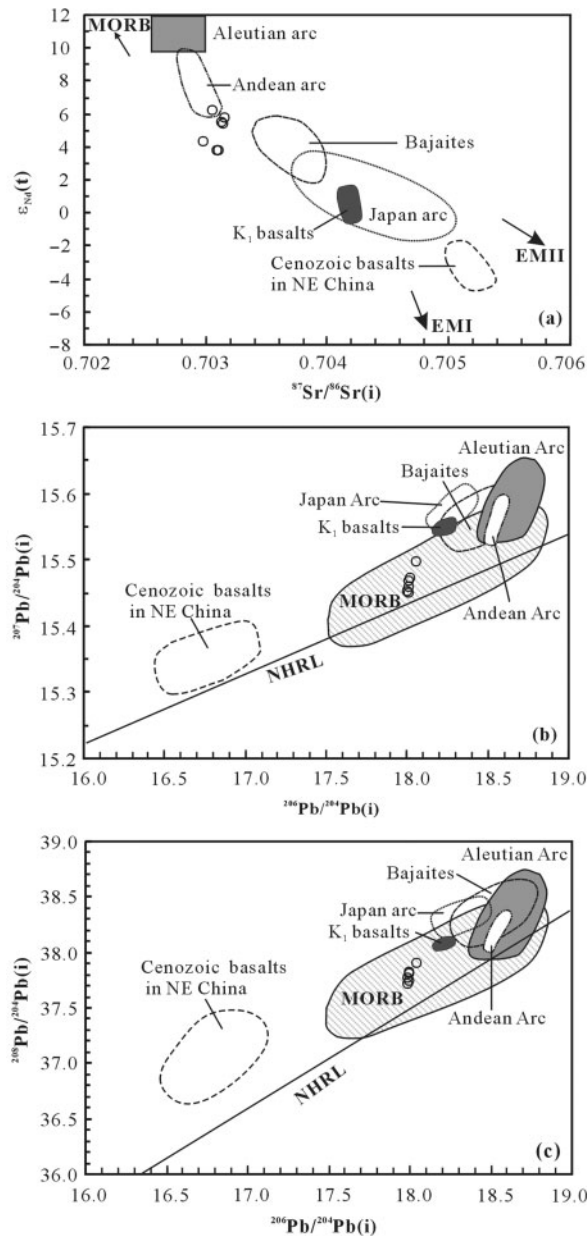


Fig. 13. Sr–Nd–Pb isotope compositions of the Yanji adakitic andesites. Comparison data sources: Cenozoic basalts in NE China from Zhang *et al.* (1995); MORB from Hart (1984); magnesian andesites from the Aleutian Arc from Yögodzinski *et al.* (1995); HMAs from the Japan Arc from Shimoda *et al.* (1998) and Tatsumi (2006); bajaites from Baja California from Rogers *et al.* (1985), Saunders *et al.* (1987) and Calmus *et al.* (2003); adakites from the Andean Arc from Kay *et al.* (1993) and Stern & Kilian (1996); K₁ basalts are the early Cretaceous basalts in the Yanji area (our unpublished data). NHRL, Northern Hemisphere Reference Line (Hart, 1984).

mantle-derived (Yögodzinski & Kelemen, 1998; Calmus *et al.*, 2003; Martin *et al.*, 2005).

The high Mg-number clinopyroxenes have lower Na₂O and higher Mg-number than clinopyroxene phenocrysts in

Table 10: Zircon Hf isotopic composition in sample 04YJ-6

Spot	¹⁷⁶ Yb/ ¹⁷⁷ Hf	¹⁷⁶ Lu/ ¹⁷⁷ Hf	¹⁷⁶ Hf/ ¹⁷⁷ Hf ± 2σ	ε _{Hf} (t)	T _{DM} (Hf)	f _{Lu/Hf}
1	0.0220	0.00076	0.282822 ± 37	5.91	606	-0.977
2	0.0579	0.00198	0.282896 ± 47	8.38	518	-0.940
3	0.0420	0.00140	0.282714 ± 40	2.01	771	-0.958
4	0.0165	0.00058	0.282793 ± 41	4.90	644	-0.983
5	0.0187	0.00065	0.282914 ± 43	9.16	476	-0.981
6	0.0827	0.00282	0.282761 ± 54	3.49	732	-0.915
7	0.0246	0.00082	0.282964 ± 38	10.91	407	-0.975
8	0.0176	0.00062	0.282792 ± 49	4.86	646	-0.981
9	0.0137	0.00047	0.282813 ± 38	5.63	614	-0.986
10	0.0297	0.00096	0.282867 ± 44	7.47	546	-0.971
11	0.1447	0.00480	0.283018 ± 61	12.34	369	-0.855
12	0.0197	0.00069	0.282860 ± 40	7.26	552	-0.979
13	0.0159	0.00057	0.282886 ± 42	8.18	514	-0.983
14	0.0273	0.00107	0.282826 ± 37	6.01	605	-0.968
15	0.0166	0.00065	0.282978 ± 17	11.46	384	-0.981
16	0.0115	0.00048	0.282902 ± 15	8.76	490	-0.986
17	0.0163	0.00059	0.282927 ± 17	9.66	456	-0.982
18	0.0133	0.00047	0.282927 ± 17	9.66	455	-0.986
19	0.0752	0.00241	0.282943 ± 20	9.98	455	-0.927
20	0.0333	0.00130	0.282986 ± 19	11.64	380	-0.961
21	0.0145	0.00055	0.282843 ± 16	6.67	574	-0.983
22	0.0138	0.00049	0.282929 ± 18	9.72	452	-0.985
23	0.0140	0.00050	0.282941 ± 15	10.15	436	-0.985
24	0.0163	0.00059	0.282907 ± 14	8.94	484	-0.982
25	0.0091	0.00034	0.282935 ± 17	9.95	442	-0.990
26	0.0180	0.00065	0.282941 ± 17	10.14	437	-0.980
27	0.0238	0.00085	0.282980 ± 17	11.48	384	-0.974
28	0.0129	0.00048	0.282940 ± 18	10.11	437	-0.986

The initial Hf isotopic ratios [ε_{Hf}(t)] are recalculated to 190 Ma. f_{Lu/Hf} = ¹⁷⁶Lu/¹⁷⁷Hf_s/¹⁷⁶Lu/¹⁷⁷Hf_{CHUR} - 1, ¹⁷⁶Lu/¹⁷⁷Hf_{CHUR} = 0.0332.

basalts (Fig. 4b). They also have higher Sr/Y and Nd/Yb_{CN} ratios than clinopyroxene from basalts in the Aleutian Arc (e.g. Yögodzinski & Kelemen, 1998). Accordingly, we suggest that the mantle-derived melt from which the clinopyroxene crystallized and that eventually mixed with the lower crustal andesitic–dacitic magma was not an arc basalt. Instead, the general positive correlation between Sr (not shown), Sr/Y, Nd/Yb_{CN} and Mg-number (Fig. 7) suggests that the mantle-derived melt had extremely high Sr, high MgO (Mg-number) and LREE/HREE ratio, but low Y and HREE concentrations, features typical of bajaites, Aleutian Adak-type magnesian andesites and other low-Si (high Mg-number) adakites (Rogers *et al.*, 1985; Kay *et al.*, 1993; Yögodzinski *et al.*, 1995; Stern & Kilian, 1996; Calmus *et al.*, 2003; Martin *et al.*, 2005).

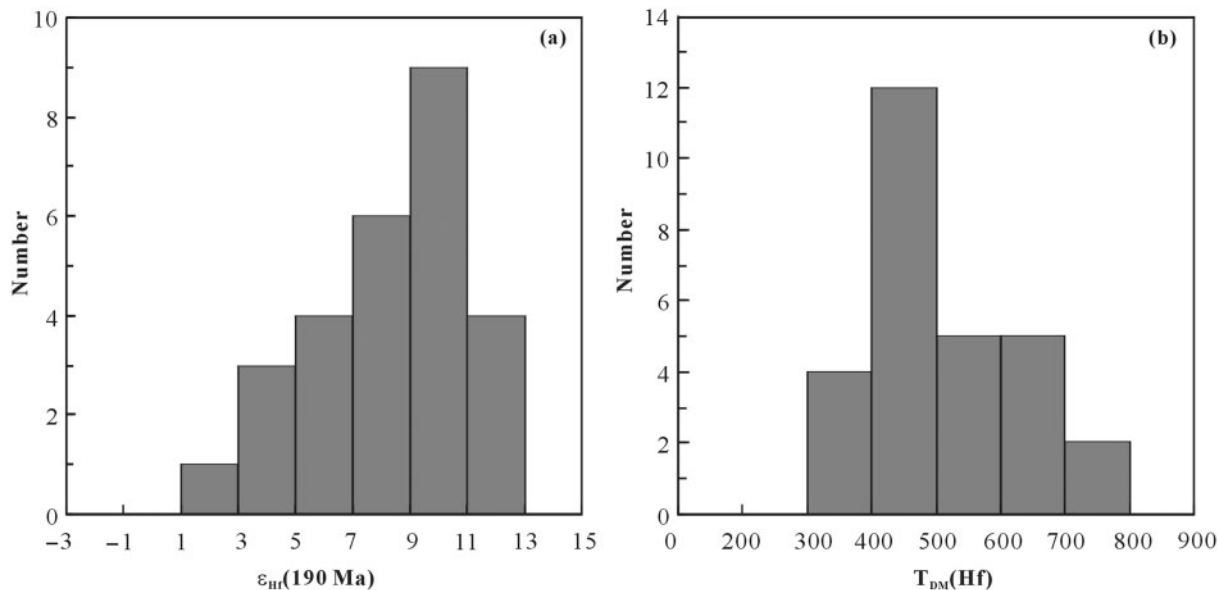


Fig. 14. Zircon Hf isotopic compositions in the Yanji adakitic andesites, NE China. (a) Histogram of zircon $\epsilon_{\text{Hf}}(t)$; (b) histogram of zircon $T_{\text{DM}}(\text{Hf})$.

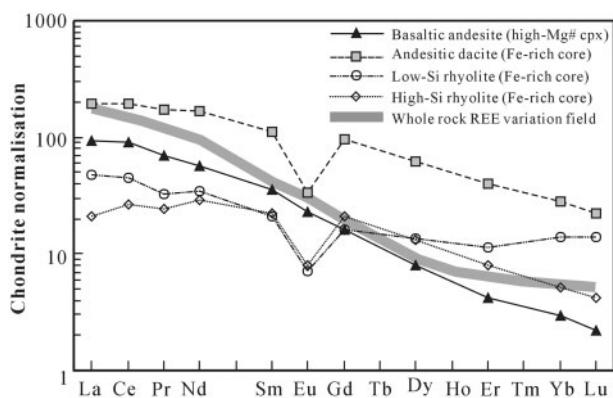


Fig. 15. Comparison between recalculated REE contents of melts respectively in equilibrium with Fe-rich clinopyroxene cores and high Mg-number clinopyroxene and the whole-rock REE concentrations of the Yanji adakitic andesites. The REE partition coefficients of clinopyroxene in equilibrium with different melt compositions and end-member components are listed in Table 11.

Thus, despite the strong evidence for magma mixing with a crustal melt, both the parental mantle-derived melt, and the post-mixing derivative Yanji adakitic andesite were high Mg-number adakitic magmas, as suggested by mixing calculation results that show that <10% felsic melt was involved in the mixed magma (Fig. 7). This is also reflected in the whole-rock isotopic data, which show MORB-like Sr, Nd and Pb isotopic compositions, suggesting that the mantle source for the high Mg-number melt was characterized by unradiogenic Sr and radiogenic Nd and Pb isotopic compositions, and that the addition

of the felsic component had only a small effect on these compositions. Considering the younger bulk $T_{\text{DM}}(\text{Nd})$ (284–442 Ma), the mantle source of these magmas was probably influenced by either contemporaneous or recent oceanic slab subduction.

Crustal contamination recorded by zircon

As recorded by the weak and normal zoning in clinopyroxene phenocrysts, the mixed magma probably accumulated in a magma chamber where it underwent differentiation before eruption. During storage or ascent through the crust, the mixed magma experienced further crustal contamination, as reflected in the zircon data, as follows (1) All zircons have much older apparent $^{206}\text{Pb}/^{238}\text{U}$ ages (170–338 Ma) than the whole-rock Ar–Ar age (55–58 Ma), suggesting they are inherited from the wall-rocks instead of crystallizing in any kind of melt involved in the magma mixing process. Zircon U–Pb dating results show that the emplacement ages of granitoid intrusions in the Yanji region spanned a range from 116 to 285 Ma (Zhang *et al.*, 2004). (2) With their reasonably high Th/U ratio (~0.6), the zircons are likely to be magmatic in origin, but the stubby morphology is typical of plutonic rocks rather than of volcanic rocks. (3) The REE patterns of the zircons of different ages are LREE-depleted and HREE-enriched with significant negative Eu anomalies, arguing against inheritance from the eclogitic protolith that produced the adakitic melt. (4) These zircons have high $\epsilon_{\text{Hf}}(190 \text{ Ma})$ (+2.0 to +12.3, with an average of +8.4) and $T_{\text{DM}}(\text{Hf})$ (369–771 Ma), suggesting that there was a considerable volume of juvenile material within the crust sampled by the high Mg-number magmas—as observed in the

Table 11: Partition coefficients (K_D) and end-member components for REE modelling

	K_D										
	La	Ce	Pr	Nd	Sm	Eu	Gd	Dy	Er	Yb	Lu
Basaltic andesite	0.10	0.17	0.20	0.40	0.55	0.50	0.65	0.90	0.80	0.70	0.55
Andesitic dacite	0.12	0.25	0.3	0.57	1.04	1.00	1.02	1.55	1.40	1.2	1.13
Low-Si rhyolite	1.11	1.83	2.00	3.30	5.23	4.10	4.80	7.30	6.80	6.40	5.93
High-Si rhyolite	0.49	1.10	1.50	2.70	5.50	4.60	6.20	7.10	4.70	2.40	1.80
<i>End-member components</i>											
High Mg-no. mantle	2.24	9.43	1.90	10.46	2.99	0.70	2.14	1.83	0.56	0.33	0.03
Fe-rich core	5.54	30.04	6.64	44.05	17.78	1.89	20.45	24.51	8.92	5.63	0.63

For REE recalculation: K_D^{REE} of clinopyroxene in basaltic-andesitic melt (Dostal *et al.*, 1983); K_D^{REE} of clinopyroxene in andesitic-dacitic melt (Luhr & Carmichael, 1980); K_D^{REE} of clinopyroxene in low-Si rhyolite (Nash & Crecraft, 1985) and in high-Si rhyolite (Sisson, 1991).

Central Asian Orogenic Belt (our unpublished data). A similar case for crustal contamination, inferred by the presence of old inherited zircons, was proposed for the Cerro Pampa adakites in Argentine Patagonia (Motoki *et al.*, 2003). Thus, the clinopyroxene and plagioclase data and the inherited zircons appear to identify two independent sources of felsic material within the Yanji adakitic andesites: an early andesitic-dacitic lower crustal melt, and later, higher level contamination by wall-rock granitoids. Despite the MORB-like Sr–Nd–Pb isotopic compositions, the later crustal contamination might also contribute to the $^{87}\text{Sr}/^{86}\text{Sr}(i)$ increase from 0.70298 to 0.70342 and $^{206}\text{Pb}/^{204}\text{Pb}(i)$ increase from 17.83 to 18.07, and $\varepsilon_{\text{Nd}}(t)$ decrease from +6.93 to +3.42 in the clinopyroxene-andesites across the Yanji area (our unpublished data). Other high Mg-number adakites, such as those at Cerro Pampa and Cook Island in the Austral Volcanic Zone in the Andean Arc (Kay *et al.*, 1993; Stern & Kilian, 1996), similarly underwent moderate amounts of crustal contamination. This possibility should be carefully assessed before such rocks are interpreted as direct partial melts of either the subducting slab or slab melt-metasomatized mantle. Indeed, where contamination is more extensive or where the contaminating crust is isotopically more evolved, clear evidence for an adakitic parental magma might be lost.

To summarize the above discussion, we can depict the magmatic evolution of the Yanji adakitic andesites in the following stages (Fig. 16). (1) Generation of two kinds of magmas derived from slab-metasomatized mantle and crust, respectively. The mantle-derived magma crystallized high Mg-number clinopyroxene (possibly some Cr-diopside fragments were captured from the melting mantle source) whereas Fe-rich clinopyroxene cores and low-An plagioclase were derived from the crustal-sourced

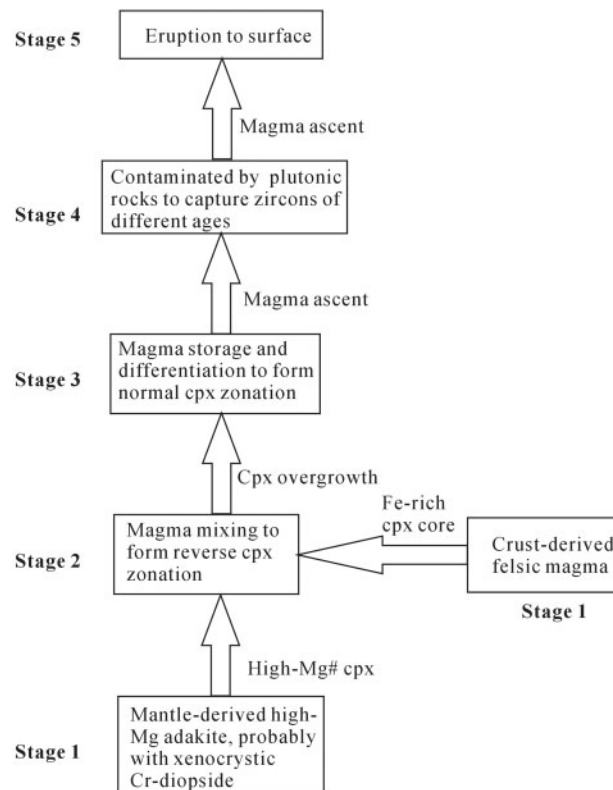


Fig. 16. A schematic diagram showing the magmatic evolution of the Palaeocene Yanji adakitic andesites. (See details in the text.)

felsic melt. (2) Mixing between the two types of magmas in a crustal magma chamber led to formation of the reverse zonation in clinopyroxene. (3) Magma storage and differentiation generated the weak to normal zonation in clinopyroxene with increasing incompatible element

concentrations at the outermost rim. (4) During magma storage or ascent, the mixed magma was further contaminated by plutonic wall rocks, leading to entrainment of zircons of a range of different ages, which possibly led to the Sr–Nd–Pb isotopic variations in these rocks.

POSSIBLE LINK WITH LATE CRETACEOUS–PALAEOCENE PACIFIC SUBDUCTION

Although the Palaeocene Yanji adakitic andesites were generated by magma mixing, the primary high Mg-number adakitic magma was derived from a LILE- and LREE-enriched mantle source metasomatized by slab melt, as envisaged for low-Si adakites defined by Martin *et al.* (2005). How and when the slab-modified mantle was formed remains unclear, as the coeval arc magmas that might place robust constraints on the enrichment event are lacking. As discussed above, the Yanji area experienced a complex evolution from the late Palaeozoic to Cenozoic, and there are three possible subduction events that might have generated the slab-modified mantle reservoir from which the primary high Mg-number adakites were derived: (1) subduction of the Palaeo-Asian ocean during the late Palaeozoic to early Mesozoic (Robison *et al.*, 1999; Jia *et al.*, 2004); (2) the late Cretaceous (95–65 Ma) Izanagi–Farallon ridge subduction associated with the formation of a Late Cretaceous accretionary prism and arc magmatism in southwestern Japan [e.g. the Shikoku accretion mélange that was subducted at around 70 Ma (Taira, 2001, and references therein)]; (3) the Kula–Pacific ridge subduction during Palaeocene times (~55 Ma), associated with the formation of the Shimanto and western Hokkaido accretionary prisms and the contemporaneous emplacement of voluminous granitic intrusions in SW and northern Japan (Maeda & Kagami, 1996; Taira, 2001).

The first possibility can be ruled out because the Palaeocene adakitic andesites have less radiogenic Pb and Sr, and more radiogenic Nd isotopic compositions than the early Cretaceous basalts (Fig. 13). Considering the effect of crustal contamination on Palaeocene adakitic magma evolution, the mantle source for the primary high Mg-number adakites must have had much lower Sr and Pb and higher Nd isotope ratios than the source for the early Cretaceous basalts. A LILE- and LREE-enriched mantle source metasomatized by slab melt will have higher Rb/Sr and lower Sm/Nd and U/Pb ratios than chondrite or Bulk Silicate Earth, and will develop more radiogenic Sr, and less radiogenic Nd and Pb isotopic compositions with time. This is the opposite of what we observe in the Yanji area. It is therefore unlikely that the Palaeocene primary high Mg-number adakitic magma originated from the same mantle source as that producing

the early Cretaceous basalts, even if the Palaeo-Asian oceanic slab-modified mantle survived into the Palaeocene.

The Palaeocene Kula–Pacific ridge subduction toward the Hidaka magmatic zone of central Hokkaido in northern Japan could have influenced the formation of the Yanji adakitic andesites (Maeda & Kagami, 1996). However, as well as the absence of coeval arc magmas in the Yanji area, field observations of Upper Cretaceous and Palaeocene sediments in this area, and in the surrounding regions, suggest that they are terrestrial deposits with coal layers, distinct from the accretionary prism deposits along the Japan Arc, which comprise mainly oceanic-plate mélanges (e.g. turbidite units, pillow lavas, radiolarian cherts, serpentinites, and high-temperature metamorphic belts; Taira, 2001, and references therein). Additionally, previous studies of the Palaeocene geology inferred an extensional regime for the Yanji area, and the surrounding regions; for example, the opening of Bohai Bay coinciding with eruption of asthenosphere-derived tholeiitic basalts in the regions along the Tanlu fault, and the rifting of the Songliao basin (Chen *et al.*, 1992; Liu, R. X., *et al.*, 1992; Liu, J. Q., *et al.*, 2001; Xu *et al.*, 1995; Wang *et al.*, 2002*b*). All these points tend to negate a direct link between the Palaeocene Yanji adakitic generation and the contemporaneous Kula–Pacific ridge subduction towards northern Japan.

Rather, we prefer to relate the generation of the Palaeocene Yanji adakitic andesites to Izanagi–Farallon ridge subduction during the late Cretaceous. According to this model, the mantle source for the primary high Mg-number adakites was formed during slab subduction, but the mantle melting event postdated the ridge subduction (Fig. 17a), analogous to the post-subduction production of magmas in Baja California (e.g. Rogers *et al.*, 1985; Saunders *et al.*, 1987). The evidence for an extensional tectonic regime in the Yanji area, and in surrounding regions, during the Palaeocene Epoch might suggest that lithospheric extension was the cause of mantle melting, production of the parental high Mg-number adakite and melting of the lower crust to form felsic melts with which the adakite magmas mixed (Fig. 17b). Such an extensional regime is also different from the ridge–trench collision setting in the Austral volcanic zone of Andean Arc, where contemporaneous slab melting occurred to form the Neogene Cerro Pampa adakites (Kay *et al.*, 1993).

Despite the proposed genetic link with the late Cretaceous (~70 Ma) Farallon–Izanagi ridge subduction that led to the LILE and LREE enrichment of the mantle source (e.g. Taira, 2001), generation of the Palaeocene Yanji adakitic andesites does not necessitate either contemporaneous subduction of a young and hot oceanic ridge and associated slab melt metasomatism, or delamination

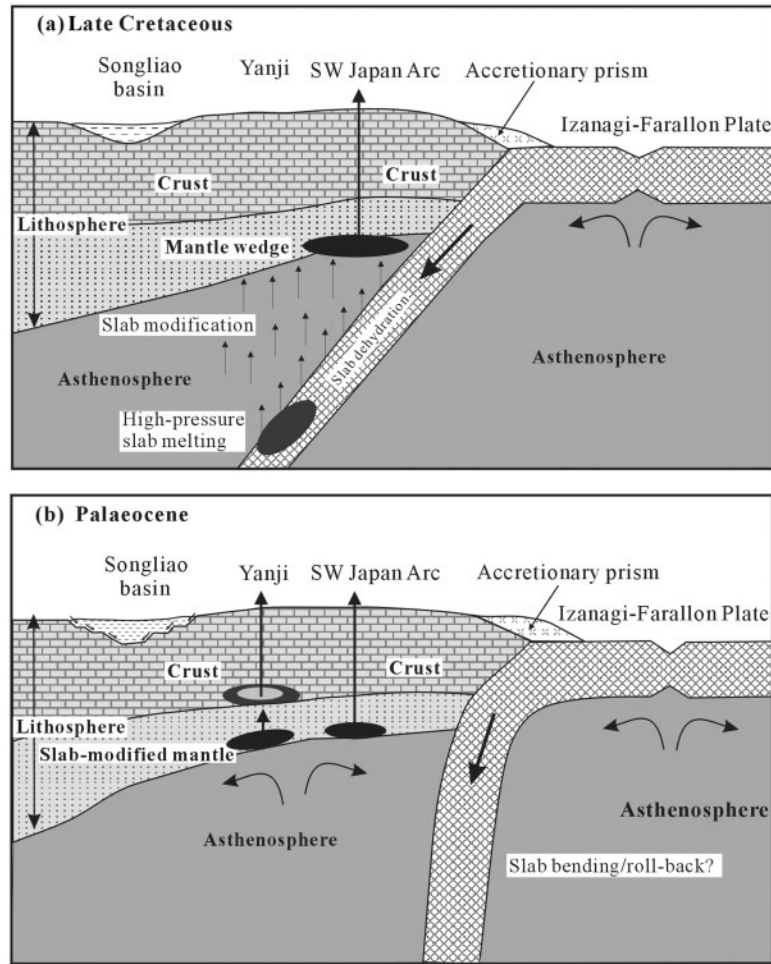


Fig. 17. A schematic illustration of the possible tectono-magmatic evolution of the Yanji area and the adjacent regions during the late Cretaceous to Palaeocene. (a) In the late Cretaceous, subduction of the Izanagi–Farallon plate beneath SW Japan caused contemporaneous arc magmatism and slab metasomatism in the overlying asthenosphere and mantle wedge (Kinoshita, 1995; Taira, 2001). (b) During the Palaeocene, bending or roll-back of the subducted slab led to asthenospheric upwelling and decompressional melting of the slab-modified mantle to produce the primary adakitic melts (Gvirtzman & Nur, 1999), which ascended and mixed with the crust-derived felsic magmas to form the Yanji adakitic andesites. (See details in the text.)

of eclogitic lower crust as suggested by previous hypotheses.

CONCLUSIONS

Palaeocene (55–58 Ma) adakitic andesites from the Yanji area, NE China, are characterized by high MgO (Mg-number), Cr and Ni, extremely high Sr, low Y and HREE concentrations, and MORB-like Sr–Nd–Pb isotopic compositions. Mineralogical evidence from clinopyroxene phenocrysts and microcrystalline plagioclase indicates an origin through mixing between a crust-derived felsic magma having high Y and HREE concentrations and low Sr, Sr/Y and Nd/Yb_{CN} ratios, and a mantle-derived high Mg-number adakitic melt.

During magma storage or ascent to surface, the mixed magma experienced crustal contamination to capture zircons from the wall-rock granitoid plutons, which possibly led to the whole-rock Sr–Nd–Pb isotopic variations. Our results support previous studies that suggest that adakitic magmas with high MgO (or Mg-number) are not necessarily near-primary melts in equilibrium with the mantle, and magmatic process including magma mixing and crustal contamination should be investigated in detail before the wider geodynamic significance of such rocks is evaluated.

The absence of coeval arc magmatism and an associated accretionary prism assemblage, together with an extensional tectonic regime in the Yanji area during the Palaeocene Epoch, suggest that adakite generation

postdated the late Cretaceous Fallaron–Izanagi ridge subduction, and is thus considered to have been produced under post-subduction extension. Generation of the Yanji adakitic andesites does not necessitate contemporaneous subduction of a young and hot oceanic ridge, slab melt metasomatism or delamination of eclogitic lower crust as suggested by previous hypotheses.

ACKNOWLEDGEMENTS

The authors wish to thank R. H. Smithies for providing constructive comments and suggestions and language help on the early version. H. F. Zhang and X. L. Xiong are thanked for discussion. F. Wang, F. K. Chen, H. N. Qiu, Y. Liu and X. F. Gao are thanked for technical assistance in mineralogical and geochemical analyses, and X. Y. Li for help with fieldwork. Thorough and constructive reviews by S. M. Kay, B. Leeman, M. Streck and an anonymous reviewer helped to improve the manuscript. Editorial handling was by John Gamble. This study was financially supported by National Natural Science Foundation of China (40373018 and 40334043), and Cooperative Research program COE-21 by the Government of Japan.

REFERENCES

- Basu, A. R., Wang, J. W., Huang, W. K., Xie, G. H. & Tatsumoto, M. (1991). Major element, REE, and Pb, Nd and Sr isotopic geochemistry of Cenozoic volcanic rocks of eastern China: implications for their origin from suboceanic-type mantle reservoirs. *Earth and Planetary Science Letters* **105**, 149–169.
- Bindeman, I. N., Eiler, J. M., Yogodzinski, G. M., Tatsumi, Y., Stern, C. R., Grove, T. L., Portnyagin, M., Hoernle, K. & Danyushevsky, L. V. (2005). Oxygen isotope evidence for slab melting in modern and ancient subduction zones. *Earth and Planetary Science Letters* **235**, 480–496.
- Calmus, T., Aguilón-Robles, A., Maury, R. C., Bellon, H., Benoit, M., Cotton, J., Bourgeois, J. & Michaud, F. (2003). Spatial and temporal evolution of basalts and magnesian andesites ('bajaites') from Baja California, Mexico: the role of slab melts. *Lithos* **66**, 77–105.
- Chen, F. K., Satir, M., Ji, J. & Zhang, D. (2002). Nd–Sr–Pb isotopes of Tēngchong Cenozoic volcanic rocks from western Yunnan, China: evidence for an enriched mantle source. *Journal of Asian Earth Sciences* **21**, 39–45.
- Chen, W. J., Li, D. M., Li, Q., Shen, S. W., Liang, H. D., Zhou, X. H., Liu, R. X., Wang, X., Liu, X. T. & Zheng, J. W. (1992). The age and geochemistry of basin basalts at Xialiaohe rift. In: Liu, R. (ed.) *The Age and Geochemistry of Cenozoic Volcanic Rocks in China*. Beijing: Seismological Press, pp. 44–80 (in Chinese).
- Compston, W., Williams, I. S. & Mayer, C. (1984). U–Pb geochronology of zircons from Lunar Breccia 73217 using a Sensitive High Resolution Ion Microprobe. *Proceedings of the XIV Lunar and Planetary Science Conference. Journal of Geophysical Research* **89** (Supplement), B525–B534.
- Compston, W., Williams, I. S., Kirschvink, J. L., Zhang, Z. C. & Ma, G. G. (1992). Zircon U–Pb ages for the Early Cambrian time scale. *Journal of the Geological Society, London* **149**, 171–184.
- Defant, M. J. & Drummond, M. S. (1990). Derivation of some modern arc magmas by melting of young subducted lithosphere. *Nature* **347**, 662–665.
- Dostal, J., Dupuy, C., Carron, J. P., Le Guen de Kerneizon, M. & Maury, R. C. (1983). Partition coefficients of trace elements: application to volcanic rocks of St Vincent, West Indies. *Geochimica et Cosmochimica Acta* **47**, 525–533.
- Engebretson, D. C., Cox, A. & Gordon, R. G. (1985). Relative motions between oceanic and continental plates in the Pacific basins. *Geological Society of America, Special Papers* **206**, 1–59.
- Fan, W. M., Guo, F., Wang, Y. J. & Lin, G. (2003). Late Mesozoic calc-alkaline volcanism of post-orogenic extension in the northern Da Hinggan Mountains, northeastern China. *Journal of Volcanology and Geothermal Research* **121**, 115–135.
- Faure, M. & Natal'in, B. (1992). The geodynamic evolution of the eastern Eurasian margin in Mesozoic times. *Tectonophysics* **208**, 397–411.
- Green, T. H. (1982). Anatexis of mafic crust and high pressure crystallization of andesites. In: Thorpe, R. S. (ed.) *Andesites: Orogenic Andesites and Related Rocks*. Chichester: John Wiley, pp. 465–487.
- Griffin, W. L., Wang, X., Jackson, S. E., Pearson, N. J., O'Reilly, S. Y., Xu, X. S. & Zhou, X. M. (2002). Zircon chemistry and magma mixing, SE China: in-situ analysis of Hf isotopes, Tonglu and Pingtan igneous complexes. *Lithos* **61**, 237–269.
- Gvirtzman, Z. & Nur, A. (1999). The formation of Mount Etna as the consequence of slab rollback. *Nature* **401**, 782–785.
- Guo, F., Fan, W. M. & Li, C. W. (2006). Geochemistry of late Mesozoic adakites from the Sulu belt, eastern China: magma genesis and implications for crustal recycling beneath continental collisional orogens. *Geological Magazine* **143**, 1–13.
- Hanyu, T., Tatsumi, Y. & Nakai, A. (2002). A contribution of slab melts to the formation of high-Mg andesite magmas: Hf isotopic evidence from SW Japan. *Geophysical Research Letters* **29**, 81–84.
- Hart, S. R. (1984). A large-scale isotope anomaly in the southern hemisphere mantle. *Nature* **309**, 753–757.
- Hirose, K. (1997). Melting experiments on lherzolite KLB-1 under hydrous conditions and generation of high-magnesian andesitic melts. *Geology* **25**, 42–44.
- Jia, D. C., Hu, R. Z., Lu, Y. & Qiu, X. L. (2004). Collision belt between the Khanka block and the North China block in the Yanbian Region, Northeast China. *Journal of Asian Earth Sciences* **23**, 211–219.
- Jilin Bureau of Geology and Mineral Resources (JBGMR) (1988). *Regional Geology of Jilin Province*. Beijing: Geological Publishing House, 698 pp. (in Chinese with English summary).
- Kamei, A., Owada, M., Nagao, T. & Shiraki, K. (2004). High-Mg diorites derived from sanukitic HMA magmas, Kyushu Island, southwest Japan arc: evidence from clinopyroxene and whole rock compositions. *Lithos* **75**, 359–371.
- Kay, R. W. (1978). Aleutian magnesian andesites-melts from subducted Pacific ocean crust. *Journal of Volcanology and Geothermal Research* **4**, 117–132.
- Kay, S. M., Ramos, C. A. & Marquez, M. (1993). Evidence in Cerro Pampa volcanic rocks for slab-melting prior to ridge–trench collision in southern South America. *Journal of Geology* **101**, 703–714.
- Kelemen, P. B. (1995). Genesis of high-Mg-number andesites and the continental crust. *Contributions to Mineralogy and Petrology* **120**, 1–19.
- Kinoshita, O. (1995). Migration of igneous activities related to ridge subduction in Southwest Japan and the East Asian continental margin from the Mesozoic to the Paleogene. *Tectonophysics* **245**, 25–35.
- Koppers, A. A. P. (2002). ArArCALC—software for $^{40}\text{Ar}/^{39}\text{Ar}$ age calculations. *Computers and Geosciences* **28**, 605–619.

- Kushiro, I. (1969). The system forsterite–diopside–silica with and without water at high pressures. *American Journal of Sciences* **267**, 269–294.
- Lee, Y. S., Ishikawa, N. & Kim, W. K. (1999). Paleomagnetism of Tertiary rocks on the Korea Peninsula: tectonic implications for the opening of the East Sea (Sea of Japan). *Tectonophysics* **304**, 131–149.
- Li, C. W., Guo, F., Fan, W. M. & Gao, X. F. (2007). Ar–Ar geochronology on Late Mesozoic volcanic rocks from the Yanji area, NE China and tectonic implications. *Science in China (Series D)* (in press).
- Liu, C. Q., Masuda, A. & Xie, G. H. (1994). Major- and trace-element compositions of Cenozoic basalts in eastern China: petrogenesis and mantle source. *Chemical Geology* **114**, 19–42.
- Liu, D. Y., Jian, P., Zhang, Q., Zhang, F. Q., Shi, Y. R., Shi, G. H., Zhang, L. Q. & Tao, H. (2003). SHRIMP dating of adakites in the Tulingkai ophiolite, Inner Mongolia: evidence for the Early Paleozoic subduction. *Acta Geologica Sinica* **77**, 317–327 (in Chinese with English abstract).
- Liu, J. Q., Han, J. T. & Fyfe, W. S. (2001). Cenozoic episodic volcanism and continental rifting in northeast China and possible link to Japan Sea development as revealed from K–Ar geochronology. *Tectonophysics* **339**, 385–401.
- Liu, R. X., Chen, W. J., Sun, J. Z. & Li, D. M. (1992). The K–Ar age and tectonic environment of Cenozoic volcanic rocks in China. In: Liu, R. (ed.) *The Age and Geochemistry of Cenozoic Volcanic Rock in China*. Beijing: Seismology Press, pp. 1–43 (in Chinese).
- Liu, Y., Liu, H. C. & Li, X. H. (1996). Simultaneous and precise determination of 40 trace element elements using ICP-MS. *Geochimica* **25**, 552–558 (in Chinese with English abstract).
- Luhr, J. F. & Carmichael, I. S. E. (1980). The Colima volcanic complex, Mexico. I: Post-caldera andesites from Volcan Colima. *Contributions to Mineralogy and Petrology* **71**, 343–372.
- Macpherson, C. G., Dreher, S. T. & Thirlwall, M. F. (2006). Adakites without slab melting: high pressure differentiation of island arc magma, Mindanao, the Philippines. *Earth and Planetary Science Letters* **243**, 581–593.
- Maeda, J. & Kagami, H. (1996). Interaction of a spreading ridge and an accretionary prism: implications from MORB magmatism in the Hidaka magmatic zone, Hokkaido, Japan. *Geology* **24**, 31–34.
- Martin, H., Smithies, R. H., Rapp, R., Moyen, J.-F. & Champion, D. (2005). An overview of adakite, tonalite–trondhjemite–granodiorite (TTG), and sanukitoid: relationships and some implications for crustal evolution. *Lithos* **79**, 1–24.
- Maruyama, S., Liou, J. G. & Seno, T. (1989). Mesozoic and Cenozoic evolution of Asia. In: Ben-Avraham, Z. (ed.) *The Evolution of the Pacific Ocean Margins*. Oxford Monograph of Geology and Geophysics **8**, 75–99.
- Motoki, A., Orihashi, Y., Cario, F. D., Hirata, D., Haller, M. J., Ramos, V. A., Kawano, H., Watanabe, Y., Schilling, M., Iwano, H. & Anma, R. (2003). U–Pb dating for single grain zircon using laser ablation ICP mass spectrometer and fission track ages for zircon grains of back-arc adakitic bodies, Argentine Patagonia. In: *The Fourth International Symposium of Isotope Geology, Abstracts*, pp. 219–220.
- Nash, W. P. & Crecraft, H. R. (1985). Partition coefficients for trace elements in silicic magmas. *Geochimica et Cosmochimica Acta* **49**, 2309–2322.
- Nakamura, E. & Kushiro, I. (1998). Trace element diffusion in jadeite and diopside melts at high pressures and its geochemical implication. *Geochimica et Cosmochimica Acta* **62**, 3151–3160.
- Nakamura, E., McCulloch, M. T. & Campbell, I. H. (1990). Chemical geodynamics in the back-arc region of Japan based on the trace element and Sr–Nd isotopic compositions. *Tectonophysics* **174**, 207–233.
- Northrup, C. J., Royden, L. H. & Burchfiel, B. C. (1995). Motion of the Pacific plate relative to Euroasia and its potential relation to Cenozoic extrusion along the eastern margin of Eurasia. *Geology* **23**, 719–722.
- Peng, Y. J. & Su, Y. Z. (1997). Geotectonic characteristics of central Jilin Province. *Memoirs of Shenyang Institute of Geology and Mineral Resources, Chinese Academy of Geological Sciences* **5–6**, 335–376 (in Chinese).
- Petford, N. & Atherton, M. P. (1996). Na-rich partial melts from newly underplated basaltic crust: the Cordillera Blanca Batholith, Peru. *Journal of Petrology* **37**, 1491–1521.
- Proureau, G., Scaillet, B., Pichavant, M. & Maury, R. C. (2001). Evidence for mantle metasomatism by hydrous silicic melts derived from subducted oceanic crust. *Nature* **410**, 197–200.
- Qiu, H. N. (2006). Construction and development of new Ar–Ar laboratories in China: insight from VG-5400 Ar–Ar laboratory in Guangzhou Institute of Geochemistry, Chinese Academy of Sciences. *Geochimica* **35**, 133–140 (in Chinese with English abstract).
- Rapp, R. P. & Watson, E. B. (1995). Dehydration melting of metabasalt at 8–32 kbar: implications for continental growth and crust–mantle recycling. *Journal of Petrology* **36**, 891–931.
- Rapp, R. P., Shimizu, N., Norman, M. D. & Applegate, G. S. (1999). Reaction between slab-derived melts and peridotite in the mantle wedge: experimental constraints at 3–8 GPa. *Chemical Geology* **160**, 335–356.
- Renne, P. R., Swisher, C. C., Deino, A. L., Owens, T. L., DePaolo, D. J. & Karner, D. B. (1998). Intercalibration of standards, absolute ages and uncertainties in $^{40}\text{Ar}/^{39}\text{Ar}$ dating. *Chemical Geology* **145**, 117–152.
- Robinson, P. T., Zhou, M. F., Hu, X. F., Reynolds, P., Bai, W. J., Yang, J. (1999). Geochemical constraints on the origin of the Hegenshan ophiolite, Inner Mongolia, China. *Journal of Asian Earth Sciences* **17**, 423–442.
- Rogers, G., Saunders, A. D., Terrell, D. J., Verma, S. P. & Marriner, G. F. (1985). Geochemistry of Holocene volcanic rocks associated with ridge subduction in Baja California, Mexico. *Nature* **315**, 389–392.
- Rubatto, D. (2002). Zircon trace element geochemistry: partitioning with garnet and the link between U–Pb ages and metamorphism. *Chemical Geology* **184**, 123–138.
- Rudnick, R. L. & Fountain, D. M. (1995). Nature and composition of the continental crust: a lower crustal perspective. *Reviews of Geophysics* **33**, 267–309.
- Saunders, A. D., Rogers, G., Marriner, G. F., Terrell, D. J. & Verma, S. P. (1987). Geochemistry of Cenozoic volcanic rocks, Baja California, Mexico: implications for the petrogenesis of post-subduction magmas. *Journal of Volcanology and Geothermal Research* **32**, 223–245.
- Sengör, A. M. C., Natal'in, B. A. & Burtman, V. S. (1993). Evolution of the Altaid tectonic collage and Paleozoic crustal growth in Eurasia. *Nature* **364**, 299–307.
- Shao, J. A. & Tang, K. D. (1995). *Terranes in Northeast China and Evolution of Northeast Asia Continental Margin*. Beijing: Seismological Press, pp. 64–70 (in Chinese with English summary).
- Shimoda, G., Tatsumi, Y., Nohda, S., Ishizaka, K. & Jahn, B. M. (1998). Setouchi high-Mg andesites revisited: geochemical evidence for melting of subducting sediments. *Earth and Planetary Science Letters* **160**, 479–492.
- Shirey, S. B. & Hanson, G. N. (1984). Mantle derived Archaean monzodiorites and trachyandesites. *Nature* **310**, 222–224.
- Sisson, T. W. (1991). Pyroxene–high-silica rhyolite trace element partition coefficients measured by ion microprobe. *Geochimica et Cosmochimica Acta* **55**, 1575–1585.

- Smithies, R. H. (2000). The Archaean tonalite–trondhjemite–granodiorite (TTG) series is not analogue of Cenozoic adakites. *Earth and Planetary Science Letters* **182**, 115–125.
- Steiger, R. H. & Jäger, E. (1977). Subcommittee on geochronology: convention on the use of decay constants in geo- and cosmo-chronology. *Earth and Planetary Science Letters* **36**, 359–362.
- Stern, C. R. & Kilian, R. (1996). Role of the subducted slab, mantle wedge and continental crust in the generation of adakites from the Austral volcanic zone. *Contributions to Mineralogy and Petrology* **123**, 263–281.
- Sun, S. S. & McDonough, W. F. (1989). Chemical and isotopic systematics of oceanic basalts: implication for mantle composition and processes. In: Saunders, A. D. & Norry, M. J. (eds) *Magmatism in the Ocean Basins. Geological Society London: Special Publications* **42**, 313–345.
- Taira, A. (2001). Tectonic evolution of the Japanese Island Arc system. *Annual Review of Earth and Planetary Sciences* **29**, 109–134.
- Tatsumi, Y. (2006). High-Mg andesites in the Setouchi volcanic belt, southwestern Japan: analogy to Archean magmatism and continental crust formation? *Annual Review of Earth and Planetary Sciences* **34**, 467–499.
- Tatsumi, Y., Shukuno, H., Sato, K., Shibata, T. & Yoshikawa, M. (2003). The petrology and geochemistry of high-Mg andesites at the western tip of the Setouchi volcanic belt, SW Japan. *Journal of Petrology* **44**, 1561–1578.
- Taylor, S. R. & McLennan, S. M. (1995). The geochemical evolution of the continental crust. *Reviews in Geophysics* **33**, 241–265.
- Tsuchiya, N., Suzuki, S., Kimura, J. I. & Kagami, H. (2005). Evidence for slab melt/mantle reaction: petrogenesis of Early Cretaceous and Eocene high-Mg andesites from the Kitakami Mountains, Japan. *Lithos* **79**, 179–206.
- Wang, F., Zhu, R. X., Li, Q., He, H. Y., Luo, Q. H., Lu, X. X., Sang, H. Q. & Wang, Y. L. (2004). A differential uplifting of Qinling orogeny belt evidences from $^{40}\text{Ar}/^{39}\text{Ar}$ thermochronology of granites. *Earth Science Frontier* **11**, 445–459 (in Chinese with English abstract).
- Wang, K. L., Chung, S. L., Chen, C. H. & Chen, C. H. (2002a). Geochemical constraints on the petrogenesis of high-Mg basaltic andesites from the Northern Taiwan Volcanic Zone. *Chemical Geology* **182**, 513–528.
- Wang, P. J., Liu, W. Z., Wang, S. X. & Song, W. H. (2002b). $^{40}\text{Ar}/^{39}\text{Ar}$ and K/Ar dating on the volcanic rocks in the Songliao basin, NE China: constraints on stratigraphy and basin dynamics. *International Journal of Earth Sciences* **91**, 331–340.
- Williams, I. S. (1998). U–Th–Pb geochronology by ion microprobe. In: McKibben, M. A., Shanks, W. C. & Ridley, W. I. (eds) *Applications of Microanalytical Techniques to Understanding Mineralizing Processes. Reviews in Economic Geology* **7**, 1–35.
- Xiao, W. J., Windley, B., Hao, J. & Zhai, M. G. (2003). Accretion leading to collision and the Permian Solonker suture, Inner Mongolia, China: termination of the Central Asian Orogenic Belt. *Tectonics* **22**(6), 1069, doi:10.1029/2002TC001484.
- Xiong, X. L., Adam, J. & Green, T. H. (2005). Rutile stability and rutile/melt HFSE partitioning during partial melting of hydrous basalt: implications for TTG genesis. *Chemical Geology* **218**, 339–359.
- Xiong, X. L., Xia, B., Xu, J. F., Niu, H. C. & Xiao, W. S. (2006). Na depletion in modern adakites via melt/rock reaction within the sub-arc mantle. *Chemical Geology* **229**, 273–292.
- Xu, P., Wu, F. Y., Xie, L. W. & Yang, Y. H. (2004). Hf isotopic compositions of the standard zircons for U–Pb dating. *Chinese Science Bulletin* **49**, 1642–1648.
- Xu, Y. G. (2002). Evidence for crustal components in the mantle and constraints on crustal recycling mechanisms: pyroxenite xenoliths from Hannuoba, North China. *Chemical Geology* **182**, 301–322.
- Xu, Y. G., Fan, W. M. & Lin, G. (1995). Lithosphere–asthenosphere interaction: a comparative study on Cenozoic and Mesozoic basalts around Bohai Area. *Geotectonica et Metallogenia* **19**, 1–13.
- Yamaji, A. (1990). Rapid intra-arc rifting in Miocene Northeast Japan. *Tectonics* **9**, 365–378.
- Yogodzinski, G. M. & Kelemen, P. B. (1998). Slab melting in the Aleutians: implications of an ion probe study of clinopyroxene in primitive adakite and basalt. *Earth and Planetary Science Letters* **158**, 53–65.
- Yogodzinski, G. M., Kay, R. W., Volynets, O. N., Koloskov, A. V. & Kay, S. M. (1995). Magnesian andesite in the western Aleutian Komandorsky region: implications for slab melting and processes in the mantle wedge. *Geological Society of America Bulletin* **107**, 505–519.
- Zhang, M., Suddaby, P., Thompson, R. N., Thirlwall, M. F. & Menzies, M. A. (1995). Potassic volcanic rocks in NE China: geochemical constraints on mantle source and magma genesis. *Journal of Petrology* **36**, 1275–1303.
- Zhang, Y. B., Wu, F. Y., Wilde, S. A., Zhai, M. G., Lu, X. P. & Sun, D. Y. (2004). Zircon U–Pb ages and tectonic implications of ‘Early Paleozoic’ granitoids at Yanbian, Jilin Province, northeast China. *Island Arc* **13**, 484–505.